MULTI-TARGET TRACKING VIA NONLINEAR LEAST SQUARES USING DOPPLER MEASUREMENTS FROM A PASSIVE RADAR SYSTEM

A Thesis
Presented to
The Academic Faculty

by

Sujay S. Joshi

In Partial Fulfillment
of the Requirements for the Degree
Master of Science in Electrical and Computer Engineering

Georgia Institute of Technology
May 2007

MULTI-TARGET TRACKING VIA NONLINEAR LEAST SQUARES USING DOPPLER MEASUREMENTS FROM A PASSIVE RADAR SYSTEM

Approved by:

Dr. Aaron Lanterman, Advisor
School of Electrical and Computer Engineering
Georgia Institute of Technology

Dr. Phil West
Georgia Tech Research Institute
Georgia Institute of Technology

Dr. Doug Williams
School of Electrical and Computer Engineering
Georgia Institute of Technology

Date Approved: April 6, 2007

ACKNOWLEDGEMENTS

I wish to thank Dr. Lanterman and Dr. West for their direction, insightful guidance, and positive encouragement throughout my thesis experience, in addition to giving me the great opportunity to conduct research in target tracking through the Georgia Tech Research Institute. I would also like to thank Dr. Landgren for his guidance and help when I first started my GRA in 2005. And most importantly, I have to thank my father and mother without whose constant encouragement and positive reinforcement I would have never made it this far.

TABLE OF CONTENTS

LIST OF TABLES

LIST OF FIGURES

LIST OF SYMBOLS AND ABBREVIATIONS

λ	FM radio wavelength
λ	Constant parameter for Levenberg-Marquardt algorithm
X_o	Initial target state vector
AWGN	Additive White Gaussian Noise
DOA	Direction of Arrival
EKF	Extended Kalman Filter
L-M	Levenberg-Marquardt
LSE	Least squares estimation
NLSE	Nonlinear least squares estimation
PCR	Passive covert radar
SNR	Signal-to-noise ratio
TDOA	Time difference of arrival

SUMMARY

A passive radar system's opportunistic ability to exploit ambient radio signal reflections makes it ideal for covert target tracking. This strategy, referred to as passive covert radar (PCR) or passive coherent location (PCL), typically exploits FM radio or television signals from powerful local transmitters. In addition to covertness, the absence of a dedicated transmitter helps reduce costs and overall system complexity. While a variety of measurements can be used to estimate a target's position and velocity, such as time difference of arrival (TDOA) and direction of arrival (DOA), this thesis focuses on using only Doppler shift measurements to estimate a target's state.

The work presented in this thesis examines the use of Doppler shift measurements from multiple receivers to solve the target tracking and association problem. A nonlinear least squares error (NLSE) estimation technique, called the Levenberg-Marquardt (L-M) algorithm, is used to determine a target's state (position and velocity) from these Doppler shift measurements. More than one target state can potentially produce identical Doppler shift profiles. In a single-receiver, single-target scenario, it is shown that three additional ghost targets caused by symmetry produce the same Doppler shift response. These ghosts may make state estimation impossible if receive antennas are not physically positioned to block out ghost targets. While the NLSE technique tends to give an accurate solution (state estimate) in one quadrant, three other solutions will symmetrically exist in each of the remaining three quadrants. The addition of either another receiver or another measurement (such as DOA) is needed to break this quadrant ambiguity. This thesis considers adding multiple receivers to accurately associate and track multiple targets.

Two target association methods (sequential and simultaneous) are developed, and their computational requirements and accuracy are compared. Statistical analysis of each method is conducted via Monte Carlo simulations. A grid-aided L-M search technique is investigated in an attempt to provide a better initial target state "guess" to these target association and tracking algorithms. This improved initial estimate can help the NLSE algorithm converge to a more accurate state estimate.

The analysis and simulation results suggest it is feasible to perform multi-target association and tracking using Doppler shift as the sole measurement. Both of the proposed methods gave optimal target association and converged to reasonably accurate state estimates in most of the Monte Carlo runs. The target associations and state estimates obtained from these procedures can be used to initialize a real-time tracking algorithm, such as an extended Kalman filter (EKF), to perform track maintenance.

In summary, the PCR tracking and association problem is considered for multiple targets and multiple receiver/transmitter pairs using only Doppler shift measurements. The number of targets is assumed to be fixed and it is assumed that all targets produce responses at all receivers. Two different target association and tracking methods are introduced and compared via Monte Carlo simulation.

CHAPTER 1

INTRODUCTION

1.1 Introduction to Bistatic Radar

The idea of bistatic radar has been around for many years, dating back to 1933 with Albert Taylor's patent describing the necessary equipment required to successfully implement a bistatic radar system [1]. Howland [2] describes bistatic radar as consisting of a transmitter and receiver "separated by a distance that is comparable with the expected maximum range of target detection."

A passive covert radar (PCR) system employs bistatic radar to track targets. A PCR system uses signals from existing local FM radio and television transmitters, instead of actively transmitting pulses to track targets [3,4]. It has been shown that signals from GPS satellites can also be used in a bistatic system [5]. Two different bistatic configurations were considered in [5]: one receiver and many transmitting satellites, or one transmitting satellite and multiple receivers. A bistatic radar target tracking system based on LEOS communication satellite was considered in [6]. A bistatic system consisting of a space-based radar transmitter and a stationary ground receiver was described in [7].

Strategically placed receivers collect reflected signals and attempt to determine the location and trajectory of targets in the scene. By taking advantage of these transmitters of opportunity, the system does not expend any energy, thereby allowing the system to operate covertly [8]. The earliest known implementation of such a system was during World War II by the German military, using the British radar network as the active transmitter [9]. Today, Lockheed Martin's Silent Sentry technology is one of the

most well known PCR systems. Silent Sentry has successfully demonstrated this technology on different types of aircraft, such as helicopters, surveillance and fighter aircraft, and even ballistic missiles [10].

The greatest advantage of a PCR system is that it is undetectable because of its passive nature. Another inherent advantage of exploiting these existing transmissions is that costs are considerably reduced since equipment associated with actively transmitting signals is not required. It is expected that the accuracy will increase significantly (to an extent) as the number of receivers and/or transmitters employed increases. Designing PCR systems is challenging since the reflected signal's power is often weak compared with the direct signal from the transmitter (sometimes up to 130 dB lower), which significantly reduces tracking effectiveness if complex (and potentially expensive) techniques are not employed [11,12]. Figure 1.1 [13] shows the physical bistatic PCR system simulated in this thesis.

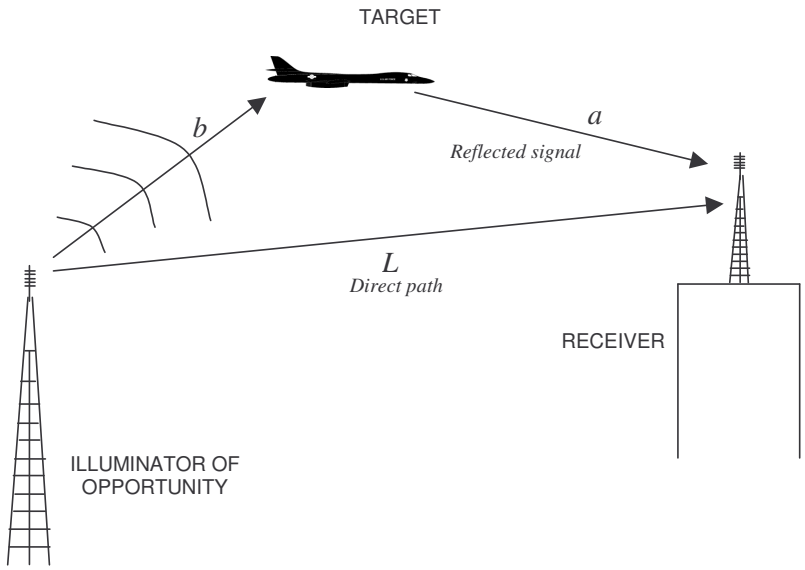

Figure 1.1: Physical layout of the bistatic PCR system for the one-target, one receiver case.

1.2 Tracking and Association Using Doppler Measurements

Howland [2] states that target tracking in a passive radar system usually relies on three measurements: TDOA, DOA, and Doppler shift. The TDOA measurement is based on finding the time difference between the reflected signal's arrival and the direct signal's arrival. The instantaneous TDOA can be calculated with the equation

$$\tau_k = \frac{1}{c}[a + b - L], \tag{1.1}$$

where c is the speed of light, a is the distance from the receiver to the target, b is the distance from the transmitter to target, and L is the direct path distance between the transmitter and the receiver [14]. The instantaneous DOA for a constant velocity target is [2]

$$\Phi[nT] = \tan^{-1}\left(\frac{x_o + nT\dot{x}}{y_o + nT\dot{y}}\right), \tag{1.2}$$

where (x_o,y_o) is the initial position of the target, T is the sampling period, n is the sample number, and $\dot{x}$ and $\dot{y}$ are the velocities in the x and y direction, respectively (assumed to be constant). The DOA measurement examines the change in angle as a function of time. At least two stationary receivers are needed for targets to be unambiguously tracked with DOA measurements [2].

The Doppler shift [2] can be expressed as

$$F_d = -\frac{1}{\lambda}\left[\frac{da}{dt} + \frac{db}{dt}\right], \tag{1.3}$$

where λ denotes the radar wavelength. The Doppler shift relies on the rate of change in the sum of the transmitter-to-target and target-to-receiver path lengths.

The available equipment limits the kind of observations that can be made. For example, if only one omnidirectional receive antenna is available (as in the case considered here), the use of angle measurements (i.e., DOA) is automatically ruled out, thereby leaving Doppler shift and TDOA as the only two available measurements.

The primary goal of this thesis is to investigate target tracking and association methods using only Doppler shift data, in both single and multi-target scenarios. The objective is to determine whether Doppler data alone is sufficient to unambiguously locate targets with a single transmitter-receiver pair, in addition to developing and comparing different multi-target tracking and association schemes and techniques. While Howland [2] uses an L-M NLSE algorithm to perform target tracking using both Doppler and DOA measurements, the contribution of this thesis is that it addresses the multi-target/multi-sensor association and tracking problem with only Doppler measurements. Like Howland [2], this thesis focuses exclusively on the L-M NLSE algorithm for estimating a target's state. In an attempt to better initialize the L-M algorithm, a grid-based search technique is explored. Since there are many outstanding issues that need to be addressed with the available hardware, the work here is all simulation-based. The eventual goal is to test the algorithms on real data.

1.3 Overview of the Thesis

As previously mentioned, the goal of this research is to accurately estimate a target's state as well as optimally associate the multiple targets over multiple receivers. In this thesis, algorithms and simulation results are presented with the hope of efficiently completing these tasks using only Doppler measurements. Chapter 2 gives a brief overview of the system, including a more in-depth look at the Doppler shift equation used

in this research. Additionally, a feasibility study regarding signal-to-noise ratio (SNR) and received power is performed to determine whether the FM and television transmitters in the local Atlanta area are strong enough to serve as passive transmitters. Basic LSE theory is also presented, along with an overview of the L-M NLSE estimation algorithm. Also, noise models used throughout the simulations are described.

Chapter 3 examines the single-receiver, single-target case and explores the symmetry involved when trying to detect the target's state. A mathematical proof of the existence of multiple solutions is presented. A grid-based NLSE technique is proposed to help achieve a more accurate target state estimate for initializing the L-M procedure. Simulation results are presented to determine the expected accuracy of the grid-aided technique.

Chapter 4 discusses two methods for multi-target tracking and association. A sequential approach and a simultaneous approach are presented, and their computational complexities, in addition to their accuracy, are compared. Both methods require multiple receivers. The sequential method considers all possible receiver orders, while the simultaneous approach considers all possible combinations in a multi-target, multi-receiver scenario. Monte Carlo simulations are conducted to determine the statistical performance of the two approaches.

Chapter 5 discusses conclusions and briefly examines future considerations for trying to improve efficiency and accuracy in these tracking and association algorithms.

CHAPTER 2

SYSTEM OVERVIEW AND FEASIBILITY ANALYSIS

This chapter describes the formulation of the target tracking problem in a two-dimensional (2-D) setting using Doppler shift measurements. The derivation of Doppler shift measurements is briefly presented in Section 2.1. In accordance with the eventual goal of implementing these target tracking and association algorithms into actual hardware experiments, a feasibility study concerning signal-to-noise ratio (SNR) and received power is performed in Section 2.2 using actual characteristics of local FM radio stations in the Atlanta area. Section 2.3 reviews LSE theory and a solution procedure based on the Levenberg-Marquardt (L-M) algorithm. Quantization error in the Doppler measurements, which results from the bin size of the discrete Fourier transform, is discussed in Section 2.4, along with an additive white Gaussian noise (AWGN) model. Section 2.5 describes the assumptions made in this thesis. Finally, examples of simulated target trajectories are presented in Section 2.6.

2.1 The Doppler Shift Measurement

The Doppler shift of a reflected signal is related to the rate of the change of the distance between the receiver and target and the distance between the transmitter and target [2]. Since this thesis considers only Doppler shift observations, it is important to briefly review the derivation of this equation. The Doppler shift can be computed as [2]

$$F_d = -\frac{1}{\lambda}\left[\frac{da}{dt} + \frac{db}{dt}\right], \tag{2.1}$$

where λ denotes the transmitted wavelength, and *a*, *b* denote the distances from the target to the receiver and the transmitter, respectively. Let the position and velocity vectors of the target be represented as

$$\vec{p} = \begin{bmatrix} x \\ y \end{bmatrix}, \tag{2.2}$$

$$\dot{\vec{p}} = \begin{bmatrix} \dot{x} \\ \dot{y} \end{bmatrix} = \begin{bmatrix} v_x \\ v_y \end{bmatrix}, \tag{2.3}$$

respectively. The distances *a* and *b* are expressed as

$$a = \left\| \vec{p} - \vec{p}_r \right\| = \sqrt{(x - x_r)^2 + (y - y_r)^2}\ , \tag{2.4}$$

$$b = \left\| \vec{p} - \vec{p}_t \right\| = \sqrt{(x - x_t)^2 + (y - y_t)^2}\ , \tag{2.5}$$

where $[x_r \ \ y_r]^T = \vec{p}_r$ represents the receiver position and $[x_t \ \ y_t]^T = \vec{p}_t$ represents the transmitter position. Now, it is possible to derive an expression that describes the rate of change of the path length from the receiver to the target. From (2.4),

$$a^2 = (\vec{p} - \vec{p}_r)^T (\vec{p} - \vec{p}_r)\,.$$

Differentiating both sides with respect to *t* gives

$$2a\dot{a} = 2(\vec{p} - \vec{p}_r)^T \frac{d}{dt}(\vec{p} - \vec{p}_r)\,,$$

which yields

$$\dot{a} = \frac{(\vec{p} - \vec{p}_r)^T \dot{\vec{p}}}{a}\,. \tag{2.6}$$

Similarly, the expression for $\dot{b}$ is

$$\dot{b} = \frac{(\vec{p} - \vec{p}_t)^T \dot{\vec{p}}}{b}\,. \tag{2.7}$$

Substituting (2.6) and (2.7) into (2.1) obtains a more explicit Doppler shift equation:

$$F_d = -\frac{1}{\lambda}\left\{\left[\frac{(\vec{p} - \vec{p}_r)^T \dot{\vec{p}}}{a}\right] + \left[\frac{(\vec{p} - \vec{p}_t)^T \dot{\vec{p}}}{b}\right]\right\}. \tag{2.8}$$

All of the variables in (2.8), except for λ, $\vec{p}_t$, $\vec{p}_r$, are functions of time *t*.

2.2 SNR and Received Power Analysis

The first step in implementing a bistatic target tracking system is to investigate the feasibility of the experiment given the available equipment. It is important to determine whether the FM and television transmitters in the local area are strong enough. Several MATLAB models were developed to see if the SNR and received power were adequate for a typical target scenario (using actual parameters of local FM/television transmitters). Additionally, throughout the analyses and simulations, it was assumed that the targets are moving in a straight line at fixed altitudes.

The equations used to compute the SNR and received powers are given by [2]

$$P_r = \frac{P_t G_t G_r \lambda^2 \sigma F_t^{\,2} F_r^{\,2}}{(4\pi)^3 L_t L_r a^2 b^2}, \tag{2.9}$$

$$SNR = \frac{P_t G_t G_r \lambda^2 \sigma F_t^{\,2} F_r^{\,2}}{(4\pi)^3 K_b T_s B L_t L_r a^2 b^2}, \tag{2.10}$$

where

- P_t, G_t, G_r are the transmitted power, and the transmit and receive antenna gains
- σ is the target's bistatic radar cross section
- F_t, F_r are "cover-all" pattern factors for antenna spatial variations
- K_b, T_s, B are Boltzmann's constant, the system noise temperature, and the effective receiver bandwidth
- L_t, L_r are extraneous transmit/receive losses

- The received power (P_r) units are in Watts (W)

A few sample contour plots showing the minimum SNR, minimum received power, and minimum dynamic range for a fixed transmitter are provided in Figures 2.1-2.3. In these plots, the target position follows a grid-like pattern at an altitude of 2.7 km, which is consistent with typical aircraft altitudes around the assumed receiver locations. The SNR and received powers were calculated at each target location, (x, y). In the SNR plots, the SNR was computed at *both* receiver locations, and the minimum of the two was plotted. The minimum SNR was plotted to give insight into the worst-case system performance. The dynamic range is the ratio of the reflected path received power to the direct path received power. In these examples, a two-receiver, one-transmitter scenario is considered, where the receivers are situated at Georgia Tech's Centennial Research Building (CRB) and Cobb County Research Facility (CCRF). The local Atlanta FM radio station WRFG 89.3 MHz was used as the transmitter of opportunity in these simulations. The FCC's FMQ FM Radio Database Query [15] provided transmitter power values, in addition to the transmitter's physical characteristics (height, location, etc).

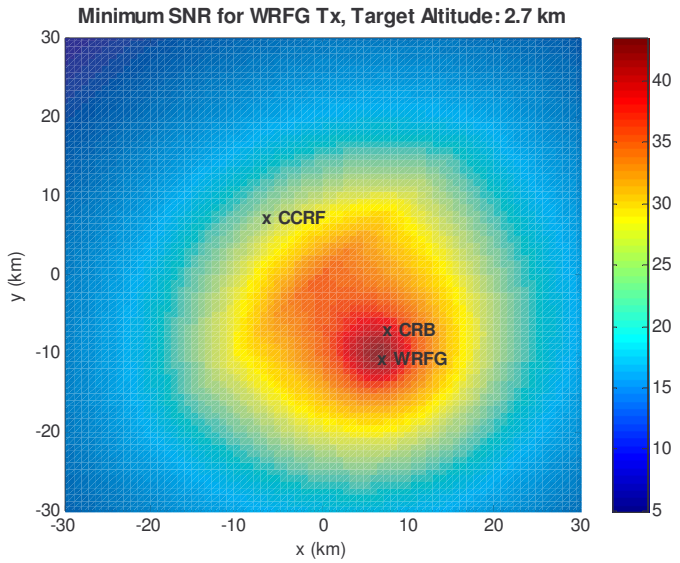

Figure 2.1. Minimum SNR of the two receivers for the one transmitter (radio station WRFG) and two-receiver (Cobb County Research Facility, Centennial Research Building) case.

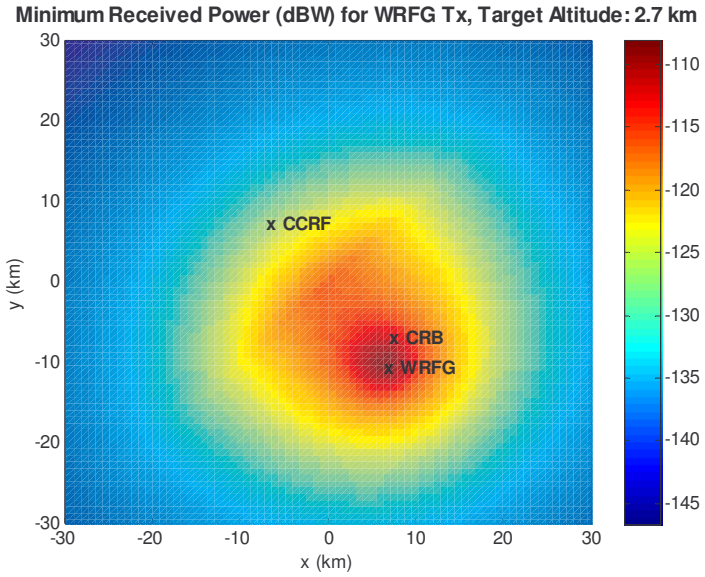

Figure 2.2 Minimum received power of the two receivers for the one-transmitter (radio station WRFG) and two-receiver (Cobb County Research Facility, Centennial Research Building) case.

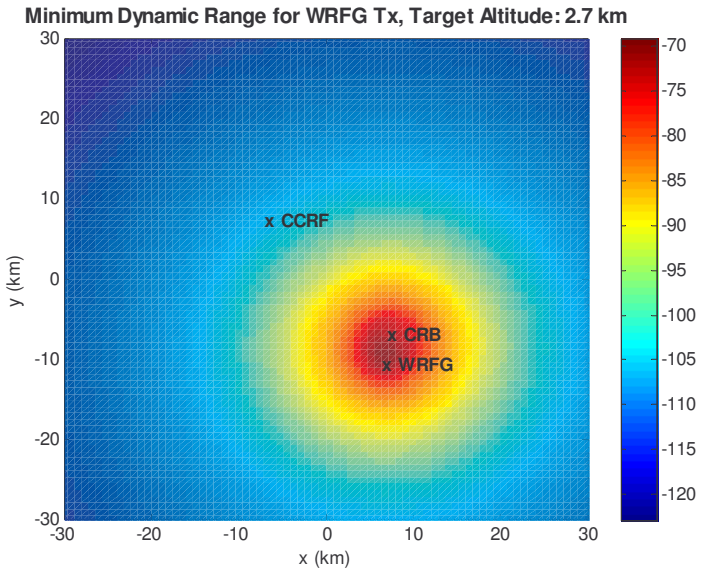

Figure 2.3. Minimum dynamic range of the two receivers for the one transmitter (radio station WRFG) and two receiver (Cobb County Research Facility, Centennial Research Building) case.

The SNR has the greatest value in the vicinity of the transmitter and the CRB, and drops at points farther away from the transmitter.

2.3 LSE and the Levenberg-Marquardt Algorithm

In LSE-based tracking [16], the current measurement and the past N–1 measurements are typically used to attain the best estimate (in the least-squares sense) of the current position and velocity. For example, consider the one-dimensional (1-D) motion of a target moving at constant velocity, v:

$$\dot{x}(t) = v \;\Rightarrow\; x(t) = x(0) + vt\,. \tag{2.11}$$

Assume that the current time is $t = (N-1)T$ and the current position is $x([N-1]T)$, where T is the sampling period.

For explanatory purposes, suppose that the measurement at time t=kT is simply

$$y_k = y(kT) = x(kT) + w_k\,, \tag{2.12}$$

where w_k is the measurement noise at time kT. Examining the N previous measurements gives

$$k=0: \quad y_0 = x_0 + w_0$$

$$k=1: \quad y_1 = x_0 + v(T) + w_1$$

$$\vdots$$

$$k=N-1: \quad y_{N-1} = x_0 + v(N-1)(T) + w_{N-1}$$

In vector-matrix notation,

$$Z_N = \begin{bmatrix} y_0 \\ y_1 \\ \vdots \\ y_{N-2} \\ y_{N-1} \end{bmatrix} = \begin{bmatrix} 1 & 0 \\ 1 & T \\ \vdots & \vdots \\ 1 & (N-2)T \\ 1 & (N-1)T \end{bmatrix} \begin{bmatrix} x_o \\ v \end{bmatrix} + \begin{bmatrix} w_0 \\ w_1 \\ \vdots \\ w_{N-2} \\ w_{N-1} \end{bmatrix}. \tag{2.13}$$

More compactly,

$$Z_N = H_N X + W, \tag{2.14}$$

where $X = [x_0, v]^T$, W is the vector of measurement noise, and H_N is the $N \times 2$ matrix on the right hand side of (2.13). The problem is to find the unknown vector X (i.e., the initial position x_o and velocity v) that minimizes the sum-squared error (cost)

$$J_{LS} = \sum_{k=0}^{N-1} [y_k - x(kT)]^2 = (Z_N - H_N X)^T (Z_N - H_N X). \tag{2.15}$$

The solution according to the linear LSE method is simply [16]

$$\hat{X} = [H_N{}^T H_N]^{-1} H_N{}^T Z_N. \tag{2.16}$$

The state estimate at the current time is obtained by propagating the initial state estimate through $(N-1)$ time steps.

The above formulation addresses the 1-D case with linear observations. However, in the case of target tracking, measurements such as Doppler shift, TDOA, and DOA are all highly nonlinear functions of the target position and velocity. Therefore, the corresponding observation equation is of the form $Z_N = h(X) + W$, where $h(\cdot)$ is a nonlinear function.

Consider the case of Doppler measurements. Here, Z_N is the actual Doppler measurement vector, while $h(X)$ is the Doppler shift calculated using the target state vector, *X*. The state equation of the target is given by

$$X_{k+1} = F\,X_k\,, \tag{2.17}$$

where, for the 2-D problem, $X = [x, v_x, y, v_y]^T$ is the state vector, and *x*, *y* denote the position and V_x, V_y, denote velocity of the target in the *x* and *y* direction, respectively. Also,

$$F = \begin{bmatrix} 1 & T & 0 & 0 \\ 0 & 1 & 0 & 0 \\ 0 & 0 & 1 & T \\ 0 & 0 & 0 & 1 \end{bmatrix}. \tag{2.18}$$

The matrix *F* is called the state transition matrix and is used to progress to the next time sample when calculating the Doppler shift response. The Doppler shift is given by (from Section 2.1)

$$F_d = -\frac{1}{\lambda}\left\{\left[\frac{(\vec{p} - \vec{p}_r)^T\,\dot{\vec{p}}}{a}\right] + \left[\frac{(\vec{p} - \vec{p}_t)^T\,\dot{\vec{p}}}{b}\right]\right\},$$

where $\vec{p} = [x\ y]^T$, $\dot{\vec{p}} = V = [v_x\ v_y]^T$. The above expression can be rewritten as

$$h(X_o,t) = -\frac{1}{\lambda}\left[\frac{(x(t)-x_t)v_x + (y(t)-y_t)v_y}{\sqrt{(x(t)-x_t)^2 + (y(t)-y_t)^2}} + \frac{(x(t)-x_r)v_x + (y(t)-y_r)v_y}{\sqrt{(x(t)-x_r)^2 + (y(t)-y_r)^2}}\right], \tag{2.19}$$

where $x(t) = x_0 + v_x t$ and $y(t) = y_0 + v_y t$. The velocities are assumed to be constant in this thesis. Denoting $h(X_o, kT)$ as $h_k(X_0)$ and including measurement noise, w_k, the Doppler shift measurement at time $t=kT$ is given by

$$z_k = h(X_0, kT) + w_k = h_k(X_0) + w_k. \tag{2.20}$$

The objective is to minimize the cost function [2]

$$J_{LS} = \sum_{k=0}^{N-1}[z_k - h_k(X_0)]^2 = [Z_N - h(X_0)]^T [Z_N - h(X_0)], \tag{2.21}$$

where

$$Z_N = [z_0 \; z_1 ... z_{N-1}]^T \tag{2.22}$$

and

$$h(X_0) = [h_0(X_0) \; h_1(X_0) .... h_{N-1}(X_0)]^T. \tag{2.23}$$

Minimizing J_{LS} with respect to X_0 gives the necessary condition

$$\left[\frac{\partial h(X_0)}{\partial X_0}\right]^T [Z_N - h(X_0)] = 0, \tag{2.24}$$

where

$$\frac{\partial h}{\partial X_0} = H_N(X_0) = \left[\frac{\partial h}{\partial x_0} \quad \frac{\partial h}{\partial v_x} \quad \frac{\partial h}{\partial y_0} \quad \frac{\partial h}{\partial v_y}\right]_{N\times 4}, \tag{2.25}$$

$$\frac{\partial h}{\partial x_0} = \left[\frac{\partial h_0}{\partial x_0} \quad \frac{\partial h_1}{\partial x_0} \quad .... \quad \frac{\partial h_{N-1}}{\partial x_0}\right]^T. \tag{2.26}$$

The other partial derivative terms are similarly defined. The term $\frac{\partial h_k}{\partial x_0}$ can be derived as

$$\frac{\partial h_k}{\partial x_0} = \frac{\partial h_k}{\partial x_k}\frac{\partial x_k}{\partial x_0} = \frac{\partial h_k}{\partial x_k}$$

$$= -\frac{1}{\lambda}\left[\frac{(y-y_r)[(y-y_r)v_x-(x-x_t)v_y]}{a^3} + \frac{(y-y_t)[(y-y_t)v_x-(x-x_t)v_y]}{b^3}\right] \quad (2.27)$$

The term $\frac{\partial h_k}{\partial v_x}$ can be derived as

$$\frac{\partial h_k}{\partial v_x} = \frac{\partial h_k}{\partial x_k}\frac{\partial x_k}{\partial v_x} + \frac{\partial h_k}{\partial v_x} = \left[\frac{\partial h_k}{\partial x_k}\right]kT - \frac{1}{\lambda}\left[\frac{x-x_r}{a} + \frac{x-x_t}{b}\right]. \quad (2.28)$$

Other partial derivative terms can be derived in a similar manner.

Equation (2.24) represents a set of four nonlinear coupled equations in four unknown elements of X_0. Unlike the linear example, there is no closed-form solution to this problem, and the solution must be obtained iteratively [16].

The L-M algorithm may provide an iterative solution [2]. The $(n+1)^{th}$ estimate of X_0 is

$$\hat{X}_{0_{n+1}} = \hat{X}_{0_n} + [H_N^T(\hat{X}_{0_n})H_N(\hat{X}_{0_n}) + \lambda I]^{-1} H_N{}^T(\hat{X}_{0_n})[z - h(\hat{X}_{0_n})], \quad (2.29)$$

where the subscript denotes the iteration number. The Nx4 Jacobian matrix H_N is a function of $\hat{X}_{0_n}$. The syllable λ is a constant parameter used to adjust the iteration step size and is in no way related to wavelength frequency calculations. We chose the L-M algorithm since this technique is known to incorporate some strengths of the steepest descent algorithm and the Gauss-Newton algorithm, both of which are nonlinear batch processing algorithms [17]. A small value of λ makes the step size larger, while a large value makes the step size smaller. A more in-depth formulation of the L-M parameters is presented in Section 4.2.1. Once a target state estimate is calculated, it can then be used

to initialize a real-time state estimation algorithm such as the EKF for performing track maintenance [18]. Alternatively, the LSE algorithm can be used with a moving window consisting of *N* consecutive Doppler measurements to generate the current position/velocity estimate. As time progresses, the result is a real-time (running) estimate of the state *X*. Another approach would be to use a growing window. As the size of the window increases such that a linear path is still applicable, the estimate's accuracy improves. A similar formulation can be used for the constant acceleration case.

2.4 Modeling System Noise

Simulated measurements were made by adding both quantization noise and thermal noise to the Doppler measurements. In typical PCR scenarios, Howland notes [2,18] that the quantization error, not the SNR, is the main cause of measurement distortion in Doppler measurements. In implementation, the discrete Fourier transform (DFT) is typically used to study the Doppler shift of the target reflections. The measured data is divided into sequential blocks, and the DFT is then taken on each of these blocks, resulting in a sample frequency spectrum, where the sample width is referred to as a *bin*. Dividing the frequency spectrum into bins results in quantization errors. The quantization error is uniformly distributed over an interval of length $\frac{1}{T}$ Hz centered at the bin center. The standard deviation of the quantization error can be shown to be $\sigma_e = \frac{1}{T\sqrt{12}}$ Hz [2]. To simulate quantization noise, a random number uniformly distributed over the interval $\left(-\frac{1}{2T}, \frac{1}{2T}\right)$ can be added to the Doppler shift at each time instant. A procedure for estimating Doppler shift from FM radio signals is given in [12]. An alternate approach to

Doppler frequency estimation is to pick the largest peak and its adjacent bins, then perform a curve fit to find the peak of the curve. This method can give more accurate results for higher SNRs.

In addition to the quantization error, additive white Gaussian noise (AWGN) can model noise-induced inaccuracies in the Doppler measurements. We assume such AWGN has a variance of 0.1 Hz^2, as assumed by Howland [2]. To simulate AWGN, a random variable with a normal distribution with a standard deviation of $\sqrt{0.1}$ Hz can be added to the Doppler shift at each time instant.

2.5 Assumptions for Simulated System

It is important to state some assumptions [2] made throughout this thesis. These underlying assumptions help simplify the analysis and simulations to a point where the results can be obtained efficiently while not compromising realism:

(1) All targets follow linear, constant velocity trajectories with no maneuvers. In the more general case of nonlinear target motion, difficulties arise when using the LSE batch estimation techniques to estimate the target's position and velocity if they are assumed to be constant. With NLSE techniques such as the L-M method, the algorithm needs a sufficient amount of time to generate an accurate estimate of the target's current state. This delay makes state estimation for accelerating targets considerably more difficult than for targets following constant velocity motion.

(2) All targets are considered to have zero vertical velocity. By assuming a system operating only in the *x*-*y* plane, Howland states that it is possible to ameliorate potential altitude estimation errors attributed to insufficient information when working with real data.

(3) Finally, the earth's surface is assumed to be uniformly flat. This assumption helps avoid some of the complexities associated with uneven terrain.

All of the simulated results presented in this thesis use the local Atlanta FM radio transmitter WRFG 89.3 MHz. It is assumed that a preprocessor eliminates false alarms or missed detections (see Howland [2] for a more in depth study of these methods).

2.6 Sample Trajectories

To maximize the intuition gained from the target tracking simulations, it is important to simulate target trajectories that mimic tracks in realistic scenarios. Two geometric trajectories are considered in this thesis: radial and tangential. The tracks are formed based on a polar coordinate system. In both of these target motion scenarios, a circle of radius r is drawn to enclose the transmitter-receiver network. In the case of a target following radial motion, a target starts at a point (r,θ) on the edge of the circle, where θ is the angle the radius makes with the horizontal axis. The target then moves radially inward toward the sensor network. Figure 2.4 shows a geometric representation of a target that follows radial motion. In the case of a tangential trajectory, a target follows a straight-line path that is tangent to the circle, touching it at the point (r,θ). Figure 2.5 shows a geometric representation of a target that follows tangential motion.

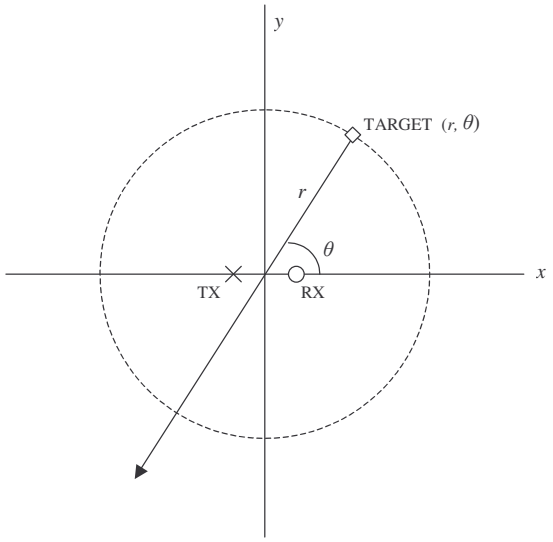

Figure 2.4. Geometric representation of a target following radial motion.

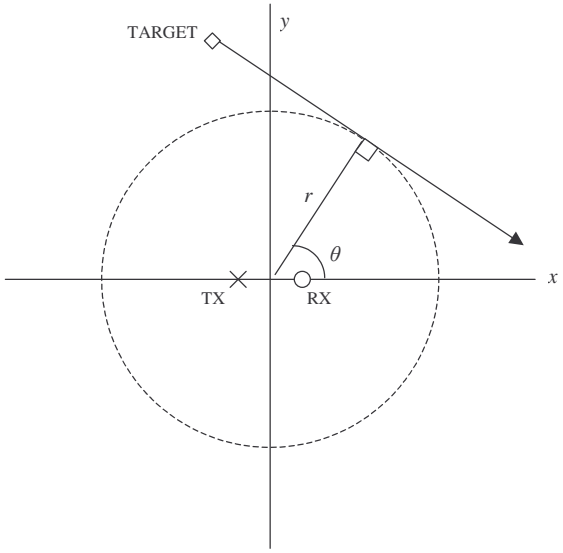

Figure 2.5. Geometric representation of a target following tangential motion.

Figure 2.6 shows four sample trajectories illustrating radial motion and their corresponding Doppler responses at constant r but varying θ. Figure 2.7 shows five

targets moving tangentially at different radii ranges r. In each figure, the angle θ is varied to show the different trajectories.

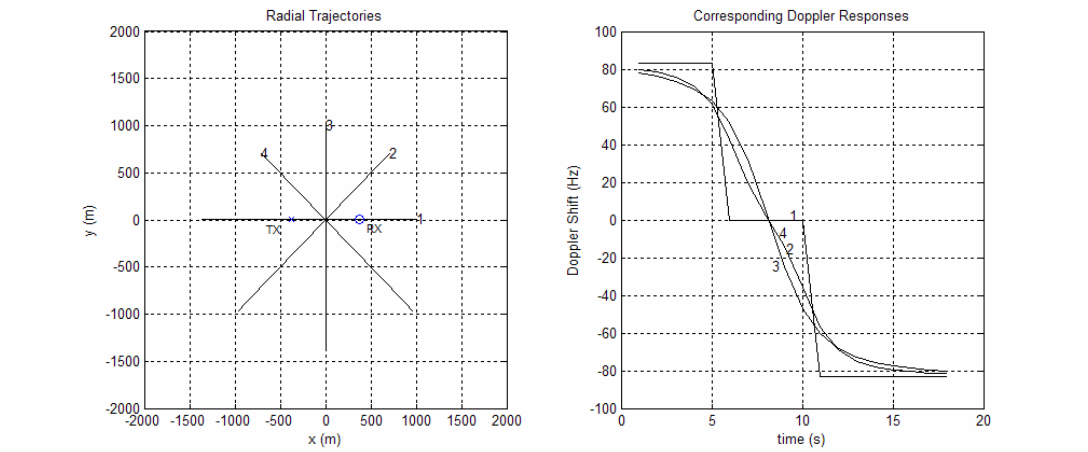

Figure 2.6. Sample trajectories for four targets following radial motion for varying θ.

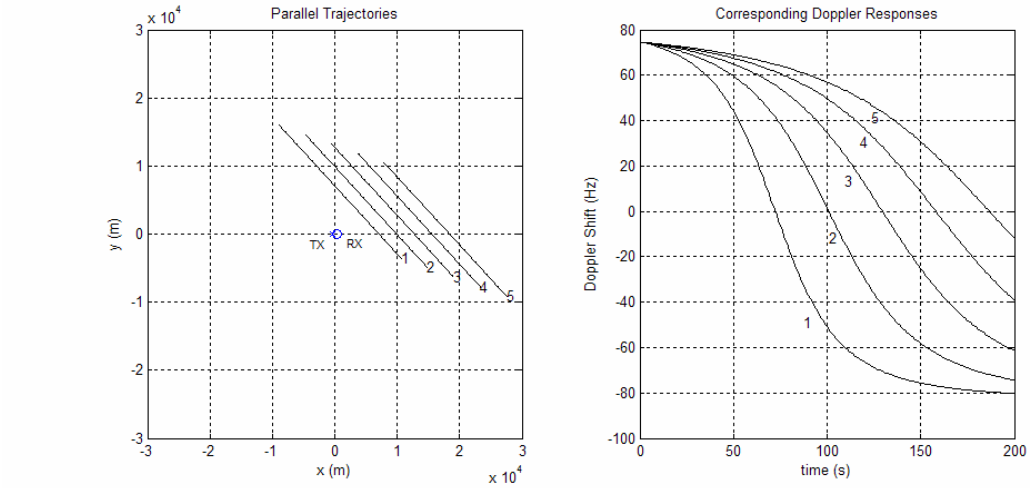

Figure 2.7. Sample trajectories for five targets moving tangentially at different radii.

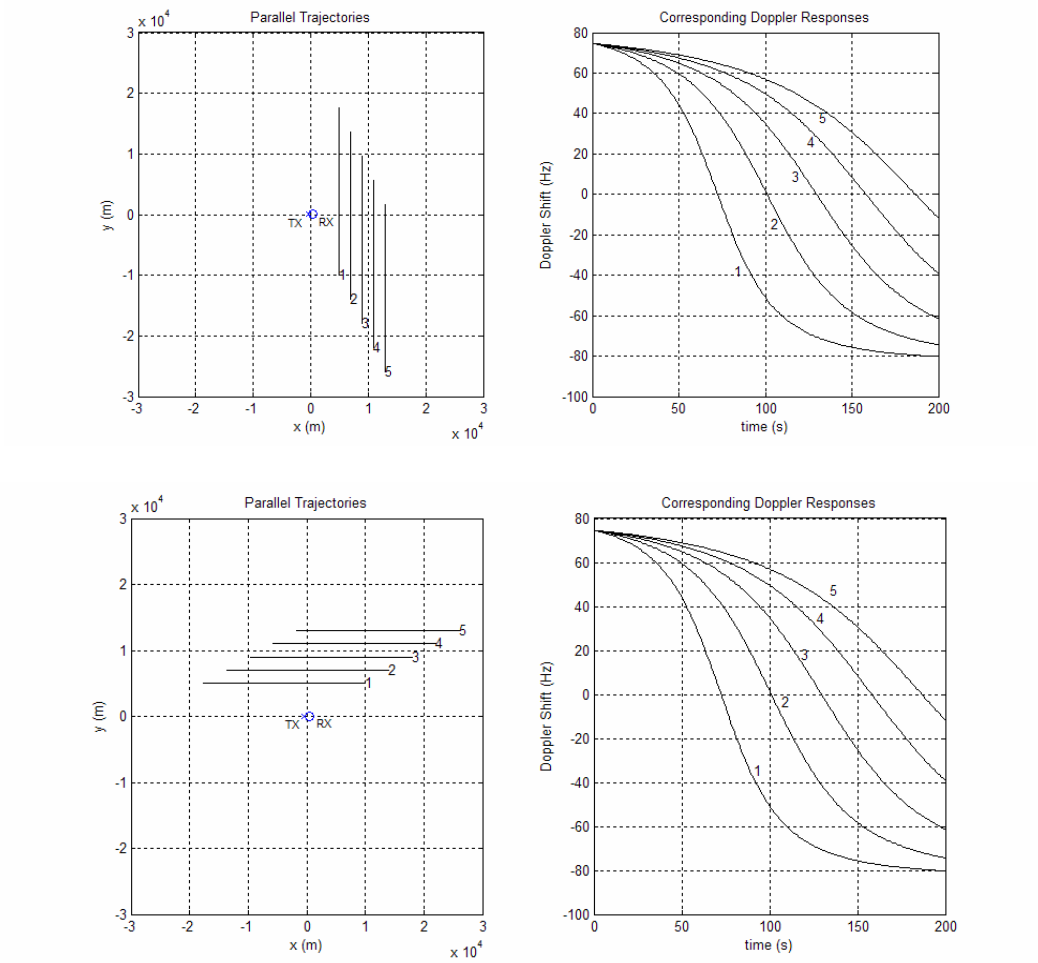

Figure 2.7 continued. Sample trajectories for five targets moving tangentially at different radii.

For tangential trajectories, the Doppler responses for the same r but different θ appear to be quite close to each other, which indicates that target state estimation would be difficult. In the case of radial trajectories, the Doppler responses for symmetric trajectories 2 and 4 overlap, which indicates that symmetric trajectories produce identical Doppler responses. Chapter 3 addresses this symmetry problem in more detail.

CHAPTER 3

SINGLE TARGET TRACKING USING DOPPLER MEASUREMENTS

This chapter addresses the basic tracking problem for a single target with one transmitter and one receiver. A one-transmitter, one-receiver scenario using just Doppler shift measurements is considered first. Early numerical results using the Levenberg-Marquardt (L-M) procedure indicated that there were multiple solutions (initial target states) that produce nearly perfect matches with the measured Doppler shift response. In-depth analysis of the problem revealed that for every initial target state, there are three additional symmetric states that produce the same Doppler shift response. The details of this symmetry property, including a mathematical proof, are presented in Section 3.1. Section 3.2 presents an example illustrating this symmetric ambiguity for a realistic trajectory. In addition, it is shown that the ambiguity due to symmetry can be resolved using an additional Doppler response at a second receiver.

The NLSE estimation method used in this thesis is based on the L-M iterative procedure [2], which usually requires a reasonably good starting guess of the initial target state. In an attempt to obtain a reasonably accurate starting guess, a grid-based search technique is studied in Section 3.3. In this procedure, a grid-shaped square pattern is created representing all of the possible target locations in the *x-y* range of interest, where at each grid point, the velocity is estimated with the L-M algorithm. By finding the target location on this grid that gives the best fit to the measured Doppler response, a better starting estimate for the full L-M algorithm that operates on both positions and velocities can be obtained.

3.1 Target Ambiguity Due to Symmetry

Without loss of generality, the coordinate system can be chosen to be centered at the midpoint of the line segment joining the transmitter and the receiver locations, with the *x*-axis defined along this line segment, and the *y*-axis defined along its perpendicular bisector. Starting with the Doppler shift equation (2.8), the Doppler shift is given by

$$F_d = -\frac{1}{\lambda}\left\{\left[\frac{(\vec{p}-\vec{p}_r)^T\,\dot{\vec{p}}}{a}\right]+\left[\frac{(\vec{p}-\vec{p}_t)^T\,\dot{\vec{p}}}{b}\right]\right\}. \tag{3.1}$$

All variables in the above equation, except for λ, $\vec{p}_r$, and $\vec{p}_t$, are functions of time *t*. The argument (*t*) has been dropped for notational convenience. This equation can be represented in terms of unit vectors by letting

$$\vec{u}_r = \frac{(\vec{p}-\vec{p}_r)}{a}, \tag{3.2}$$

$$\vec{u}_t = \frac{(\vec{p}-\vec{p}_t)}{b}, \tag{3.3}$$

where $a = \| \vec{p} - \vec{p}_r \|$ and $b = \| \vec{p} - \vec{p}_t \|$. Hence, the Doppler equation is expressed as

$$F_d = -\frac{1}{\lambda}\left[\vec{u}_r + \vec{u}_t\right]^T \dot{\vec{p}}, \tag{3.4}$$

which can be written as a dot product

$$F_d = -\frac{1}{\lambda}\left[\vec{u}_r + \vec{u}_t\right]\cdot \vec{v}, \tag{3.5}$$

where $\vec{v} = \dot{\vec{p}}$ is the target's velocity vector expressed as

$$\vec{v} = \begin{bmatrix} v_x \\ v_y \end{bmatrix}.$$

Furthermore, the dot product can be written as

$$F_d = -\frac{1}{\lambda}\left\|\vec{u}_r + \vec{u}_t\right\|\left\|\vec{v}\right\|\cos\theta, \tag{3.6}$$

where θ is the angle between the vectors $\left[\vec{u}_r + \vec{u}_t\right]$ and $\vec{v}$.

For the proceeding discussion, consider the target state

$$X_1 = \begin{bmatrix} x_o \\ v_x \\ y_o \\ v_y \end{bmatrix}. \tag{3.7}$$

There are three main types of symmetry in the 2-D target tracking problem, as defined next.

3.1.1 Axial Symmetry

The case of axial symmetry is considered first. Axial symmetry allows for a symmetric reflection about a vertical axis, where the reflected state is written as

$$X_2 = \begin{bmatrix} x_o \\ v_x \\ -y_o \\ -v_y \end{bmatrix}. \tag{3.8}$$

This target state X_2 is defined to be the axially symmetric reflection of target state X_1. Axial symmetry can be graphically represented as shown in Figure 3.1.

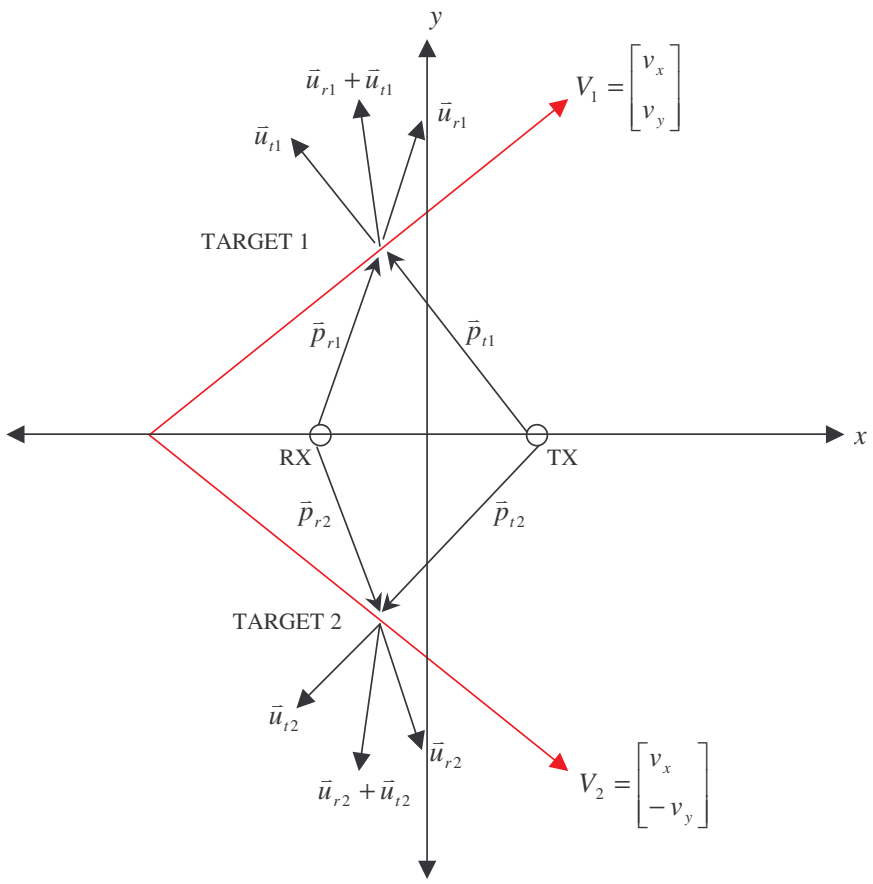

Figure 3.1. Geometric representation of axial symmetry.

3.1.2 Lateral Symmetry

In the case of lateral symmetry, the target state

$$X_3 = \begin{bmatrix} -x_o \\ -v_x \\ y_o \\ v_y \end{bmatrix} \tag{3.9}$$

is defined to be the laterally symmetric reflection of X_1. Figure 3.2 shows a graphical representation of lateral symmetry.

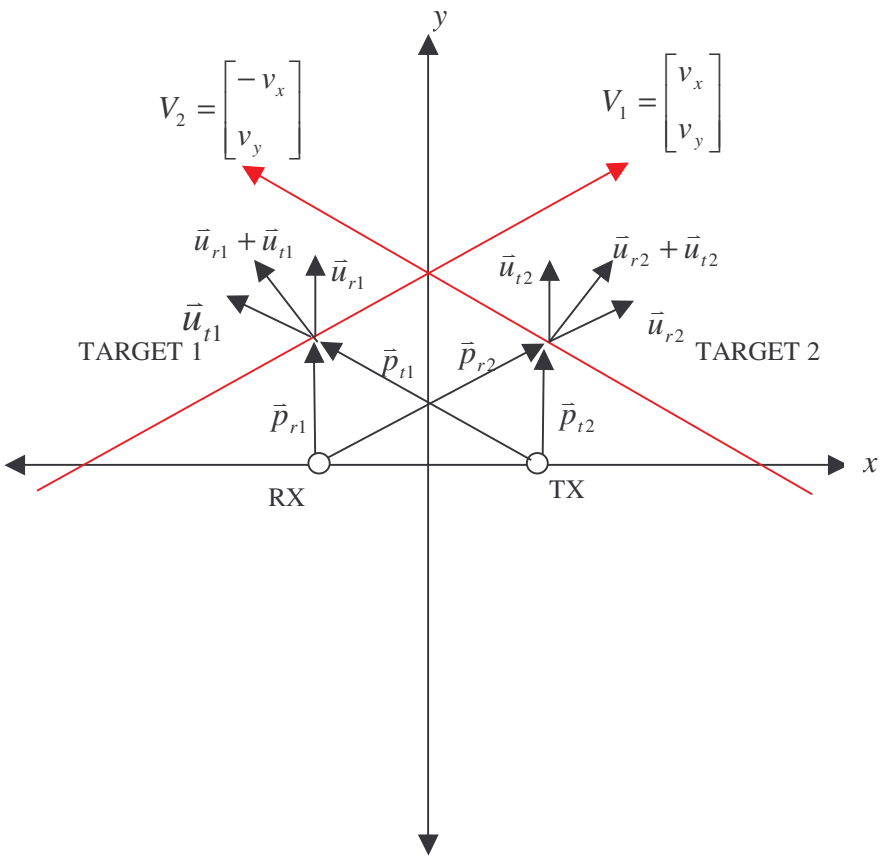

Figure 3.2. Geometric representation of lateral symmetry.

3.1.3 Odd Symmetry

Finally, with odd symmetry, the target state

$$X_4 = -X_1 = \begin{bmatrix} -x_o \\ -v_x \\ -y_o \\ -v_y \end{bmatrix} \tag{3.10}$$

is defined to be the odd symmetric reflection of X_1 (Figure 3.3).

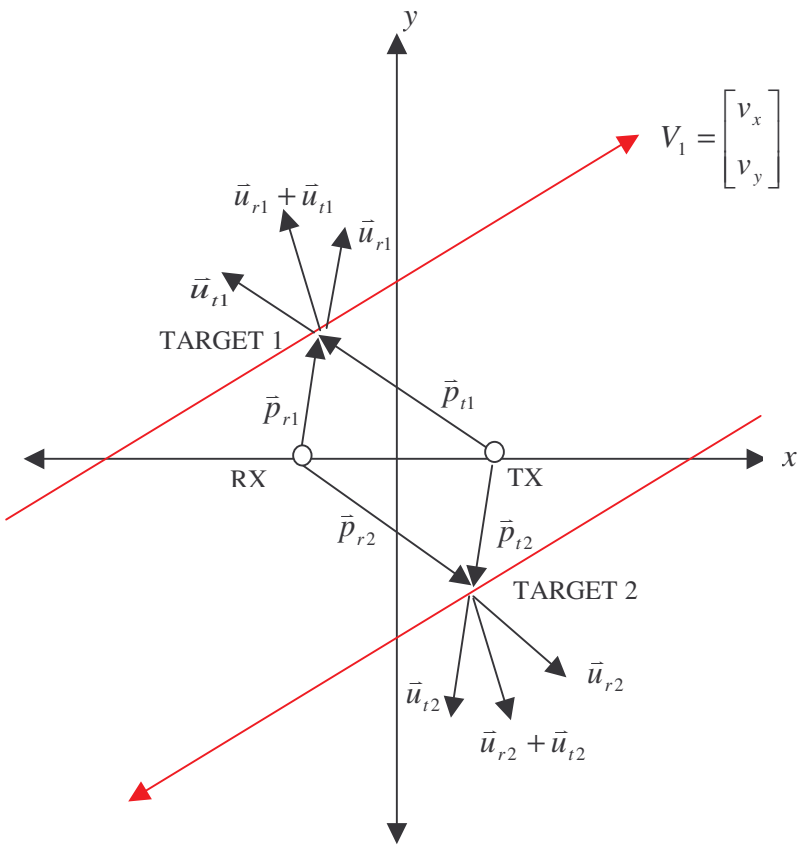

Figure 3.3. Geometric representation of odd symmetry.

It can be shown that the three symmetric reflections of the target state produce the same Doppler response. However, for brevity, only the axial symmetry case will be considered in the proof presented next.

3.1.4 Identical Doppler Responses for Symmetric Trajectories

From (3.6), the Doppler shift responses for the two targets shown in Figure 3.1 are

$$F_{d1} = -\frac{1}{\lambda}\left\|\vec{u}_{r1} + \vec{u}_{t1}\right\|\left\|\vec{v}_1\right\|\cos\theta_1, \tag{3.11}$$

$$F_{d2} = -\frac{1}{\lambda}\left\|\vec{u}_{r2} + \vec{u}_{t2}\right\|\left\|\vec{v}_2\right\|\cos\theta_2, \tag{3.12}$$

where F_{d1} and F_{d2} describe the Doppler shifts for target state 1 and 2, respectively. However, due to symmetry (see Figure 3.1),

$$\left\|\vec{u}_{r1}+\vec{u}_{t1}\right\|=\left\|\vec{u}_{r2}+\vec{u}_{t2}\right\|,$$

$$\theta_1=\theta_2.$$

Also, closer examination of the velocity vectors leads to

$$\left\|\vec{v}_1\right\|=\sqrt{{v_x}^2+{v_y}^2}=\sqrt{{v_x}^2+(-v_y)^2}=\left\|\vec{v}_2\right\|. \tag{3.13}$$

Hence, $F_{d1}=F_{d2}$ for all $t\geq 0$. This implies that two completely different target states can produce identical Doppler responses, thereby making the system unobservable. Completing the above procedure using lateral and odd symmetric reflections results in a similar finding.

The above results are clear and intuitive in the graphical vector-geometry setting, upon realizing that Doppler shift is simply a dot product. They can also be readily verified algebraically. The Doppler shift expression in (3.1) was expanded in Chapter 2 as

$$F_d(t)=-\frac{1}{\lambda}\left[\frac{(x(t)-x_t)v_x+(y(t)-y_t)v_y}{\sqrt{(x(t)-x_t)^2+(y(t)-y_t)^2}}+\frac{(x(t)-x_r)v_x+(y(t)-y_r)v_y}{\sqrt{(x(t)-x_r)^2+(y(t)-y_r)^2}}\right]. \tag{3.14}$$

Because of the choice of the coordinate system in this section, $(x_t, y_t)=(d, 0)$ and $(x_r, y_r)=(-d, 0)$, and

$$F_d(t)=-\frac{1}{\lambda}\left[\frac{(x(0)+v_xt-d)v_x+(y(0)+v_yt)v_y}{\sqrt{(x(0)+v_xt-d)^2+(y(0)+v_yt)^2}}+\frac{(x(0)+v_xt+d)v_x+(y(0)+v_yt)v_y}{\sqrt{(x(0)+v_xt+d)^2+(y(0)+v_yt)^2}}\right]. \tag{3.15}$$

For the axial symmetry case, it can be easily verified that replacing ($x(0)$, v_x , $y(0)$, v_y) by ($x(0)$, v_x , $-y(0)$, $-v_y$) leaves the Doppler shift unchanged in (3.15). Similar results hold for lateral and odd symmetry cases as well.

From the above discussion, four distinct initial states (trajectories) produce identical Doppler shift responses. Therefore, the initial target state cannot be uniquely determined from the Doppler shift response. Ensuring observability while using Doppler shift as the sole measurement can be accomplished in a variety of ways, however. The most straightforward would be to add at least one more receiver to the system. As long as the second receiver does not lie on the x- or y-axis, the symmetric reflections with respect to the two receivers will not coincide. One could achieve the same effect by adding another transmitter instead of another receiver. Additionally (or alternatively), another type of measurement could be added, such as direction of arrival (DOA). The addition of more measurements generally improves observability and enables unambiguous results. Since ($a+b$) is same for all reflections, the TDOA will be the same, and hence will not improve observability.

Since the main focus of this research is to attempt to track targets using only Doppler shift measurements, only the approach of adding another receiver to the system is considered. The next section presents a numerical example to demonstrate that the four-solution ambiguity can be broken by adding a second receiver.

3.2 Example: Symmetric Target Ambiguity and a Solution

As shown in the preceding section, the use of a single transmitter-receiver setup results in ambiguity. Three ghost targets, each of which produce identical Doppler responses, make it impossible to discern the actual target. This section demonstrates this

ambiguity with a realistic numerical example, and presents a solution of adding a second receiver in order to eliminate all ghost targets.

The first step in realistically illustrating the target ambiguity problem is to use the L-M algorithm to estimate the target's initial state. Since only one receiver is considered, the L-M algorithm will provide a solution that could either be the actual target state or three other (incorrect) ghost target states. Figure 3.4 illustrates the plan view of the sensor network and the four symmetric solutions. The actual target and its trajectory are also depicted. The target location in this example has a range of 5000 m and speed of 140 m/s. The trajectory corresponds to a tangential trajectory as illustrated in Chapter 2. To determine the target state, the L-M iterative method was applied to the Doppler response measured at Receiver 1. The starting guess of the initial target state was arbitrarily chosen as:

$$\hat{X}(0) = \begin{bmatrix} \hat{x}(0) \\ \hat{v}_x \\ \hat{y}(0) \\ \hat{v}_y \end{bmatrix} = \begin{bmatrix} 1 \\ 1 \\ 1 \\ 1 \end{bmatrix}.$$

The L-M procedure gave a solution (soln. #1) shown in Figure 3.4. The other three solutions (marked as soln. #2, #3, #4) can be obtained simply by taking symmetric reflections of solution #1. Figure 3.5 compares the actual and estimated Doppler shift responses at receiver 1 (RX1). The fit between the actual and measured Doppler responses is excellent, and all four solutions produce the same Doppler response.

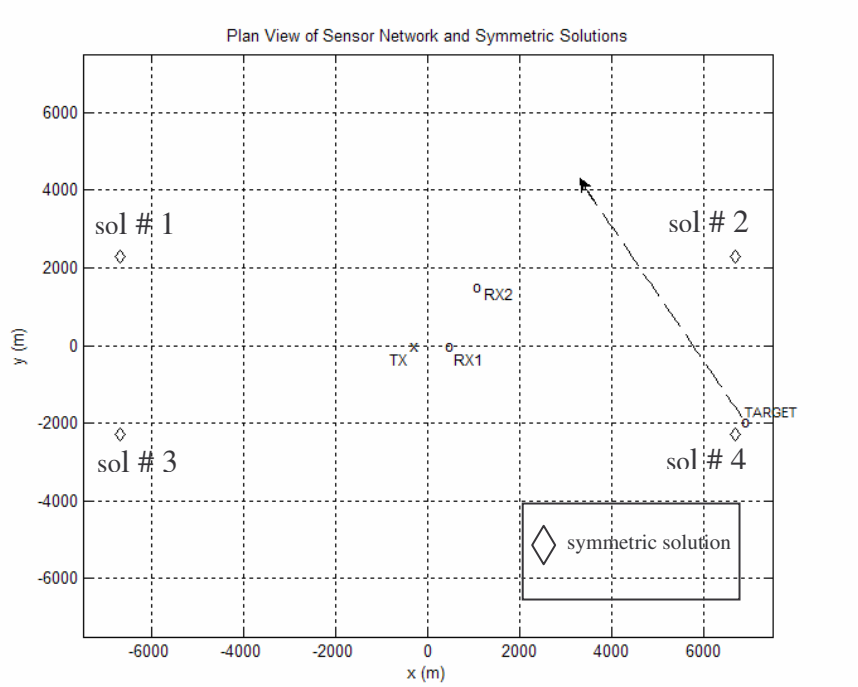

Figure 3.4. Plan view of sensor network and the four symmetric solutions.

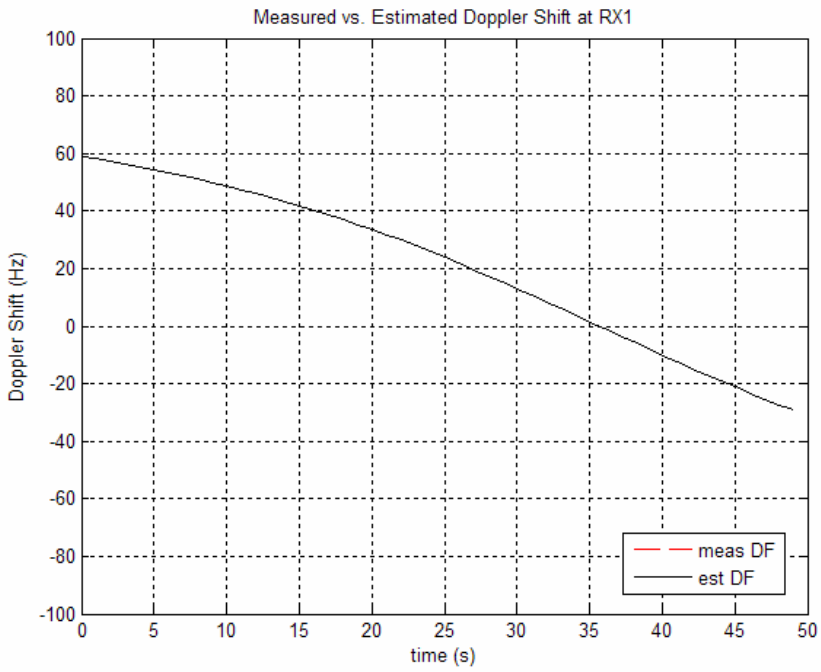

Figure 3.5. Measured vs. estimated Doppler shift responses at RX1.

Since there are four potential target states, it is impossible to determine which solution represents the actual target using just a single receiver. To break the ambiguity problem, a second receiver (RX2) is added to the sensor network as shown in Figure 3.4. Now, there are two sets of Doppler shift data that can be used to determine the actual target. The Doppler shift for each of the four symmetric states is calculated at RX2. The sum-squared difference between the actual and estimated Doppler shift (also known as the "cost") at RX2 is calculated for each symmetric solution. The cost is calculated using the formula

$$C_i = \sum_{k=0}^{N-1} \left\| m_2[k] - h_{2i}[k] \right\|^2 ,$$

where $m_2[k]$ is the actual measured Doppler shift at RX2 and $h_{2i}[k]$ is the estimated Doppler shift at RX2 produced by the i^{th} symmetric solution (i=1, 2, 3, 4). The solution that gives the smallest of the four costs is then labeled as the actual target state. The measured Doppler shift response at RX2 and the estimated Doppler shift responses for each symmetric solution at RX2 are shown in Figure 3.6. From the plots, it is easy to see that symmetric solution #4 is the actual target state. This is also confirmed by the numerical values of the costs. The final actual and estimated target states are:

$$X_o = \begin{bmatrix} x \\ \dot{x} \\ y \\ \dot{y} \end{bmatrix} = \begin{bmatrix} 6830.1 \\ -70 \\ -1830.1 \\ 121.24 \end{bmatrix} \qquad \hat{X}_o = \begin{bmatrix} x \\ \dot{x} \\ y \\ \dot{y} \end{bmatrix} = \begin{bmatrix} 6704.4 \\ -61.795 \\ -2279.9 \\ 125.75 \end{bmatrix}$$

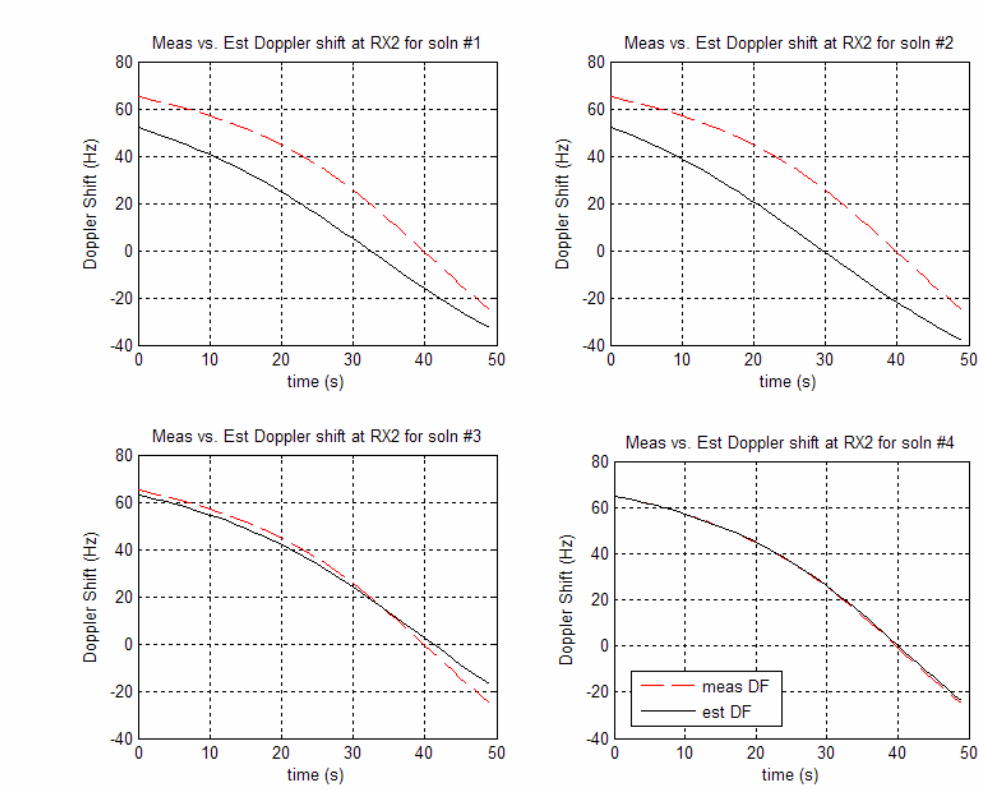

Figure 3.6. Measured vs. estimated Doppler responses at RX2 for each symmetric solution.

This example demonstrates that it is possible to effectively break the ambiguity of the solution by adding a second receiver (or transmitter). This informal approach can be methodically formalized for single and multiple targets by using data from both receivers to refine the position and velocity parameters, as will be shown in Section 4.1.

During this simulation, an arbitrary initial target state guess of [1 1 1 1] was used when running the L-M algorithm. The L-M procedure required a large number of iterations (over 2000) to produce a reasonably accurate state estimate. Additional simulation studies also indicated that the L-M algorithm with an arbitrary initial state guess either gave erroneous results or did not converge in several cases. In an attempt to

obtain a more accurate starting estimate of the target state, a grid-aided search technique is presented in the next section.

3.3 A Grid-Aided NLSE Approach

Using the L-M algorithm with an arbitrary initial state guess often results in non-convergence or an estimate that is completely different from the actual state. For the single receiver, single transmitter case, as shown in Section 3.1, there are four symmetric solutions, one in each quadrant. To help the L-M algorithm avoid getting caught in local minima because of poor initial conditions, a grid-aided search over the first quadrant can be implemented. The grid-aided method assumes an x-meter by y-meter grid spanning a portion of the first quadrant of a Cartesian plane. Within this box, the grid is broken up into a predefined number of grid points. At each grid point, the L-M algorithm estimates the x-velocity and y-velocity of the target by minimizing the sum-squared error between the actual and estimated Doppler shift while holding the position parameter fixed at the center of the grid point. This difference, also known as the "cost," is stored at each grid point. The cost is calculated using the equation

$$C_{(x,y)} = \sum_{k=0}^{N-1} \left\| m\ [k] - h_{(x,y)}[k] \right\|^2$$

where $m[k]$ is the measured Doppler shift and $h_{(x,y)}[k]$ is the estimated Doppler shift at grid point (x,y). After the algorithm has been applied to each of the grid points in the box, the minimum of all the costs is found. The (x,y) location of the grid point with the lowest cost provides the estimate of the target's position while the velocity estimated from the L-M algorithm provides the target's estimated velocity. Regardless of whether the actual target is located in the first, second, third, or fourth quadrant, the grid-aided technique

attempts to find a solution in the first quadrant by using the symmetry properties of the one-transmitter, one-receiver system scenario. Each iteration in the L-M algorithm requires only a 2x2 matrix inversion; hence the computational requirement is easily manageable. In addition, the L-M algorithm can be implemented independently and in parallel at each grid point if parallel hardware is available.

3.3.1 Example: Grid-Aided Method

Figure 3.7 shows the plan view of a grid-based field illustrating the actual target track and the L-M estimated solution for a typical target trajectory.

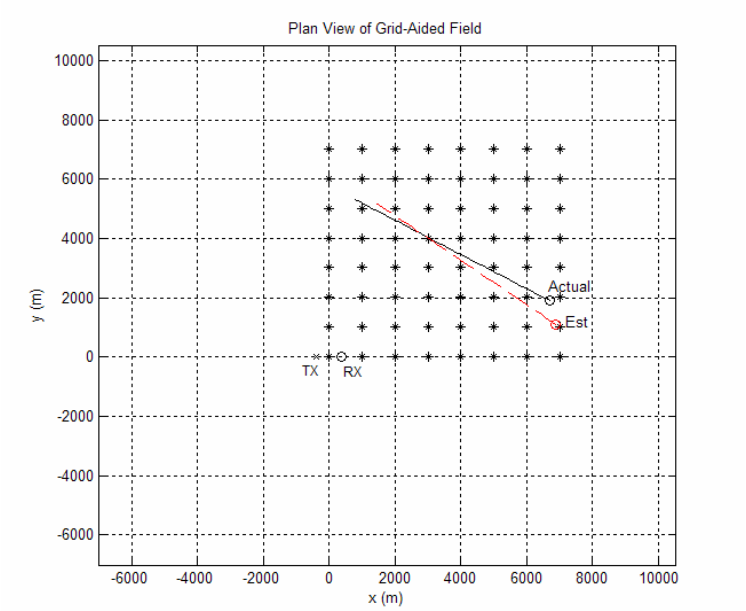

Figure 3.7. Plan view of the grid-aided method with actual and estimated trajectories.

In the example shown in Figure 3.7, a tangential target motion path with r=5000 m and $\theta = \frac{\pi}{3}$ was used. An 8x8 grid with grid points placed 1 km apart (starting at x=10 m, y=10 m) was employed. The actual and estimated states using the grid-aided method were

$$X_o = \begin{bmatrix} x \\ \dot{x} \\ y \\ \dot{y} \end{bmatrix} = \begin{bmatrix} 6380.1 \\ -121.24 \\ 1830.1 \\ 70 \end{bmatrix}, \qquad \hat{X}_o = \begin{bmatrix} x \\ \dot{x} \\ y \\ \dot{y} \end{bmatrix} = \begin{bmatrix} 7010 \\ -112.08 \\ 1010 \\ 84.006 \end{bmatrix}.$$

Using this grid-aided search technique in the first quadrant, rather than an unconstrained search over all four quadrants, allows for reduced computational run times. The target state estimate produced by the grid-aided technique can then be used as the initial state "guess" when conducting the full-state L-M estimation, as will be seen in Chapter 4.

3.3.2 Monte Carlo Simulation Results

To determine how well the grid-aided NLSE method estimates the initial target state, a Monte Carlo simulation was conducted. During this simulation, only targets that follow tangential motion were considered, where the nominal (mean) target range from the sensor network was taken as 4000 m and varied randomly with a standard deviation of 1000 m. The target speed was taken as 140 m/s. Several target location angles were randomly chosen for an initial target state in the first quadrant and a number of runs were conducted. The results show bias in the initial state estimate of

$$bias(\hat{X}_0 - X_0) = bias\begin{bmatrix} \hat{x}_0 - x_0 \\ \hat{v}_x - v_x \\ \hat{y}_0 - y_0 \\ \hat{v}_y - v_y \end{bmatrix} = \begin{bmatrix} -73.70 \\ 44.29 \\ -207.75 \\ -56.47 \end{bmatrix}.$$

Additionally, the square root mean-squared error (MSE) was

$$\sqrt{MSE}(\hat{X}_0 - X_0) = \begin{bmatrix} 797.4 \\ 53.03 \\ 1122.4 \\ 119.77 \end{bmatrix}.$$

The results show that the grid-aided method does indeed provide an initial estimate that is more accurate than arbitrarily "guessing" an initial state of [1 1 1 1]. The mean position errors obtained here are small compared to the range. The standard deviations of the *x*- and *y*-position errors are nearly 1000 m, which is the grid size. However, the means and standard deviations of the velocity errors are relatively large. In particular, the velocities are often in the wrong direction. Therefore, the position estimate obtained from the grid-aided method is used to initialize the L-M algorithm, but the initial velocity guess is taken to be zero. Multi-target tracking simulations presented in the next chapter use results obtained from the grid-aided approach as the initial conditions. These simulations rerun the L-M algorithm, using the initial conditions provided by the grid-aided study.

CHAPTER 4

MULTI-TARGET TRACKING AND ASSOCIATION USING DOPPLER MEASUREMENTS

Chapter 3 showed that single-target tracking using Doppler shift alone gives ambiguous results when using a single receiver and a single transmitter. In particular, it was shown that four distinct target states would produce identical Doppler responses. The solutions have quadrant symmetry, such that one solution lies in each of the four quadrants, causing the actual target in one quadrant to appear as a ghost in each of the other three quadrants. Therefore, it is necessary to use additional receiver(s) or transmitter(s) to determine the actual target state. Chapter 3 demonstrated that the addition of a second receiver can break the quadrant ambiguity and enable identification of the real target. The NLSE-based target state estimation employed the Levenberg-Marquardt (L-M)iterative method. The use of a grid-based search technique was investigated to help obtain a better initial state estimate for starting the full L-M procedure.

In the case of multiple targets, multiple Doppler responses will be received at each receiver, and it becomes necessary to determine target associations, that is, determine which response corresponds to which target. This chapter considers a multiple-receiver, multiple-target scenario. The objective is to determine the target associations as well as all the target states. Several example scenarios are considered: two receivers with one, two, or three targets; and three receivers with two targets. Consistent with the approach in this thesis, Doppler shift is used as the sole measurement. Although specific numbers of targets and receivers are used to demonstrate the methods and enhance

clarity, the methods are also applicable to the general case with n_t targets, n_r receivers, and n_{tx} transmitters, as long as n_t is known.

Two basic approaches to the multi-target association and tracking problem are proposed and developed in this chapter, called the "sequential method" and the "simultaneous method." The terms "sequential" and "simultaneous" refer to the way that target association is performed. Section 4.2 investigates our sequential method of target tracking and association, which makes effective use of the symmetry property of the solutions. This method is based on the preliminary procedure mentioned in Chapter 3 (Section 3.2) in which the measured Doppler shift responses at each receiver are compared with the calculated responses for all solutions (four per target) to determine the target associations and states. In Section 4.3, a simultaneous target association and tracking method is proposed that involves considering all possible combinations of Doppler shift measurements from multiple receivers, and minimizing (for each combination) the cost with respect to the initial target states of all targets simultaneously. This method simultaneously solves the target association and tracking problems, so the problem of quadrant ambiguity does not arise.

Finally, a comparison of the sequential and simultaneous methods is conducted. Numerical results from multiple Monte Carlo simulations are presented as well.

4.1 The Sequential Method

4.1.1 Procedure

The main aim of the sequential method is to ensure that two different targets are not assigned to the same measured Doppler shift data. This procedure involves sequentially

blocking out the remaining measured response and target that correspond to the lowest cost during the association process. For demonstration purposes, consider a two-receiver, three-target case. Table 4.1 shows the available measured Doppler shift data for the three targets at each of the two receivers.

Table 4.1. Measured Doppler shift data (three-target, two-receiver case).

	Meas. Doppler Shift –1	**Meas. Doppler Shift -2**	**Meas. Doppler Shift -3**
RX1	$m_{11}[k]$	$m_{12}[k]$	$m_{13}[k]$
RX2	$m_{21}[k]$	$m_{22}[k]$	$m_{23}[k]$

The first step in the sequential method is to assign the RX1 measured responses $m_{11}[k]$, $m_{12}[k]$, $m_{13}[k]$ to targets 1, 2, and 3, respectively. This can be done arbitrarily. Then, the L-M estimation algorithm is used to create target state estimates for each of the three targets using data from RX1. Chapter 3 showed this is well-facilitated by a precursory grid-aided search.

The second step is to find the other three symmetric solutions for each target. Since only one receiver was used in Step 1 to estimate the initial state, there will be three symmetric target solutions located in each of the three remaining quadrants. There are a total of 12 possible states for three targets.

The third step is to calculate the Doppler responses at receiver 2 (RX2) for all solutions of each target (four solutions per target for a total of 12 responses). The calculated Doppler response can be written as

$$\text{Calculated Doppler response} = h_2(\hat{X}_{o\_isol})\Big|_{isol=1,2,3,4},$$

where h_2 denotes the Doppler response function of RX2. Recalling (3.14), the Doppler shift equation can be expressed as

$$F_d(t) = -\frac{1}{\lambda}\left[\frac{(x(t)-x_t)v_x + (y(t)-y_t)v_y}{\sqrt{(x(t)-x_t)^2 + (y(t)-y_t)^2}} + \frac{(x(t)-x_r)v_x + (y(t)-y_r)v_y}{\sqrt{(x(t)-x_r)^2 + (y(t)-y_r)^2}}\right], \qquad (4.1)$$

where $x(t) = x(0) + v_x t,\ y(t) = y(0) + v_y t$. Each receiver response function is obtained by using the values of λ, x_r, and y_r for that receiver.

In the fourth step, each calculated Doppler response, $h_2(\hat{X}_{o\_isol})$, is compared to the measured Doppler response, $m_{2j}[k]$, for j = 1, 2, 3 and the corresponding costs are calculated. For the scenario described here, there will be 12 costs for each of the targets. Since there are three targets, there will be 36 costs.

The fifth step is to find the minimum of all of these costs. The target state estimate (one of the 12 solutions) and measured Doppler response corresponding to this lowest cost will give the optimal target state estimate for the corresponding target, as well as the optimal association.

The next few steps define the sequential technique. The measured response and target corresponding to the lowest cost (in Step 5) are blocked out so as to ensure that this state and association is not chosen again. This blocks out 12 costs. Now, the lowest of the remaining 24 costs is found and the same process (starting with Step 5) is repeated to obtain the association and state estimate of another target. Finally, of the 12 remaining costs, the lowest value is found, arriving at the final target state and its optimal association.

The steps above describe our "sequential" procedure for target association and target state estimation. To improve and refine the target state estimates by using measured responses from *both* receivers, it is critical to extend the procedure further. By incorporating data from both receivers, there is a substantially greater likelihood of

getting a more accurate state estimate for each target. In this extended process, the target associations obtained above are used to reorder the measured responses ($m_{2j}[k]$, j = 1, 2, 3) to correspond to targets 1, 2, and 3, respectively. For each target, j, the L-M method is used to minimize the cost by incorporating measured data from both receivers:

$$\sum_k (m_{1j}[k] - h_1(\hat{X}_{oj}))^2 + (m_{2j}[k] - h_2(\hat{X}_{oj}))^2 . \quad (4.2)$$

The result of this second L-M phase is expected to be a better target state estimate, $\hat{X}_{oj}$. Thus, the sequential method performs target association sequentially, but performs NLSE using data from all receivers.

Finally, note that RX1 was chosen as the first receiver in Step 1. However, it is likely that the association, and hence the tracking results, may depend on which receiver was chosen as the first receiver. To complete the procedure, the steps described above are repeated a second time with the receiver order reversed. This time the initial L-M state estimates are computed at RX2, and their Doppler responses are calculated at RX1 and compared to the measured Doppler shift at RX1 to generate the cost matrix. The association and tracking results that give the least total cost are taken to be the final results.

While considering the reversed receiver order, it should be noted that the symmetry property for the reversed receiver order holds only in the coordinate system having the x-axis collinear with the line segment joining TX and RX2, and the y-axis collinear with its perpendicular bisector. Therefore, it is necessary to perform a coordinate transformation before obtaining symmetric images of the solution.

Although the sequential method is described for a two-receiver case, it can be used with any number of receivers. However, all possible receiver orders must be considered. For n_r receivers, there are $(n_r!)$ possible orders.

4.1.2 Example: Single and Multiple Targets

One Target Case

For the single-target example, the same target motion that was defined in Chapter 3, Sec. 3.2 is considered. Figure 4.1 shows the plan view of the sensor network and the target's trajectory.

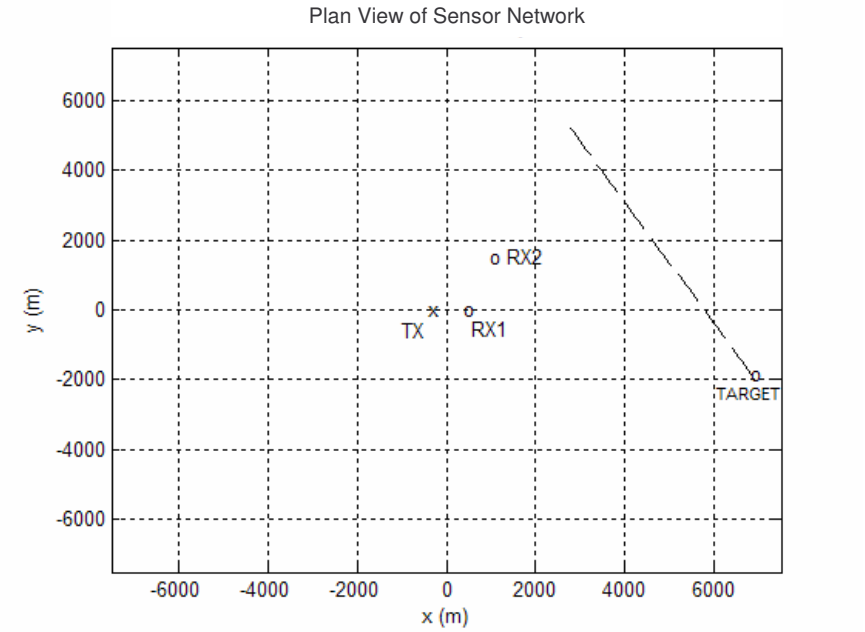

Figure 4.1. Plan view of sensor network and target trajectory via sequential method (one-target, two-receiver case).

An additive quantization error due to frequency bin size as well as an additive white channel noise were added to all Doppler measurements, as described in Chapter 2, Sec. 2.4. Recall that the sequential method uses data from both RX1 and RX2 to estimate

the target's initial state. The actual and estimated target states obtained by the sequential method were

$$X_o = \begin{bmatrix} 6830.1 \\ -70 \\ -1830.1 \\ 121.24 \end{bmatrix} \text{ and } \hat{X}_o = \begin{bmatrix} 6902 \\ -69.597 \\ -1865.1 \\ 122.49 \end{bmatrix}$$

By using data from both receivers, the sequential method provides an excellent state estimate.

Two Target Case

As an example of the two-target case, a second target was added to the scenario considered in the one-target example. Figure 4.2 shows the plan view of the sensor network and the targets' trajectories. The second target's speed is 140 m/s, and a time duration of 60 s was used with sampling interval of 1 s.

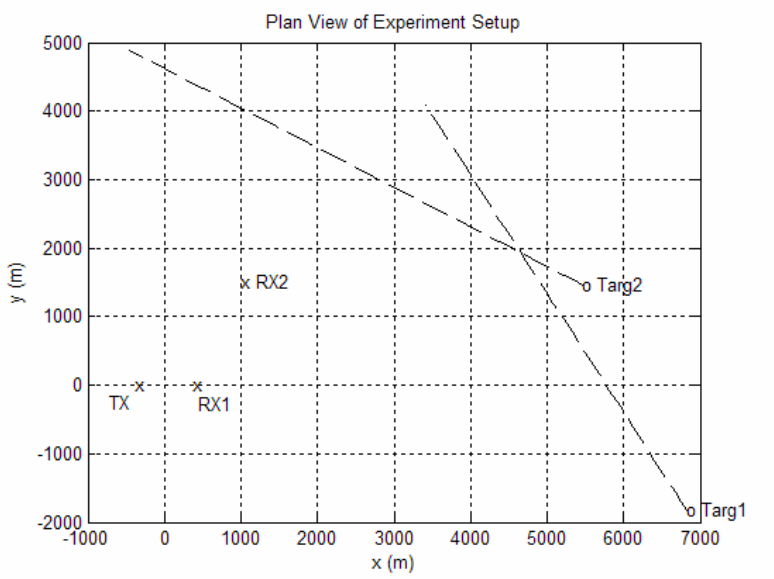

Figure 4.2. Plan view of sensor network and target trajectory via sequential method (two-target, two-receiver case).

In the two-target case, the first receiver order (RX1 taken to be the first receiver) gave better results than the second receiver order. The sequential method performed well for this case, but the time duration had to be increased to 80 s to obtain good state estimates. The actual and estimated target states for target 1 and target 2 were

$$X_{o1} = \begin{bmatrix} 6830.1 \\ -70 \\ -1830.1 \\ 121.24 \end{bmatrix} \text{ and } \hat{X}_{o1} = \begin{bmatrix} 6842.2 \\ -70.363 \\ -1813.1 \\ 121.16 \end{bmatrix}$$

$$X_{o2} = \begin{bmatrix} 5464.1 \\ -121.24 \\ 1464.1 \\ 70 \end{bmatrix} \text{ and } \hat{X}_{o2} = \begin{bmatrix} 5461.5 \\ -121.15 \\ 1458.8 \\ 70.037 \end{bmatrix}$$

Three Target Case

Figure 4.3 shows the plan view of the sensor network and the target trajectories after adding a third target, which also has a speed of 140 m/s.

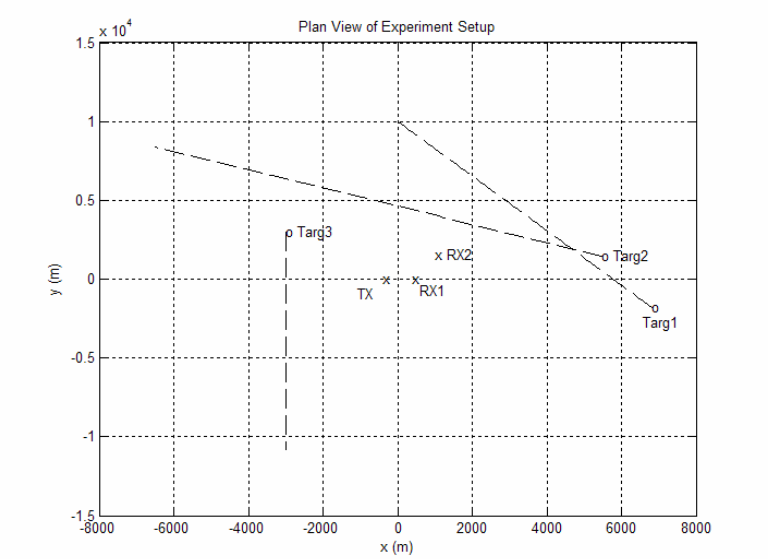

Figure 4.3. Plan view of sensor network and target trajectory via sequential method (three-target, two-receiver case).

In the three-target case, the second receiver order (i.e., RX2 taken to be the first receiver) gave better results than the first receiver order. Also the time duration had to be increased to 100 s to obtain good estimates since more information is now needed to estimate the parameters of the third target. The actual and estimated target states for target 1, 2, and 3 were

$$X_{o1} = \begin{bmatrix} 6830.1 \\ -70 \\ -1830.1 \\ 121.24 \end{bmatrix} \text{ and } \hat{X}_{o1} = \begin{bmatrix} 6829.1 \\ -69.797 \\ -1841.4 \\ 121.4 \end{bmatrix},$$

$$X_{o2} = \begin{bmatrix} 5464.1 \\ -121.24 \\ 1464.1 \\ 70 \end{bmatrix} \text{ and } \hat{X}_{o2} = \begin{bmatrix} 5460.4 \\ -121.46 \\ 1481.5 \\ 69.583 \end{bmatrix},$$

$$X_{o3} = \begin{bmatrix} -3000 \\ 0 \\ 3000 \\ -140 \end{bmatrix} \text{ and } \hat{X}_{o3} = \begin{bmatrix} -3002.7 \\ 0.117 \\ 2997.9 \\ -140.03 \end{bmatrix}.$$

As the number of targets increased, it was necessary to increase the amount of time duration needed to collect the data. By taking a sufficiently long time duration, the state estimates became close to the actual state estimates.

The examples presented in this section are intended as illustrations. The method may not successfully estimate the target state due to convergence to local minima or failure of the L-M algorithm to converge in a reasonable number of iterations. More general conclusions regarding this method's performance can be made only after a number of Monte Carlo simulations, which will be addressed in Section 4.4.

4.2 The Simultaneous Method

4.2.1 Procedure

While the sequential method minimized the cost functions in a consecutive manner, the main aim of the simultaneous method is to perform this cost-minimization together for all targets and receivers. To demonstrate the simultaneous method procedure, consider a three-receiver, two-target scenario; hence, there are two measured Doppler responses at each receiver. Let $m_{ij}[k]$ denote the j^{th} measured Doppler response at the i^{th}

receiver. Table 4.2 shows the available measured Doppler shift data for the two targets at each of the three receivers.

Table 4.2. Measured Doppler shift data for the two targets at each of the three receivers.

	Measured Doppler Shift –1	**Measured Doppler Shift -2**
RX1	$m_{11}[k]$	$m_{12}[k]$
RX2	$m_{21}[k]$	$m_{22}[k]$
RX3	$m_{31}[k]$	$m_{32}[k]$

Let the initial state estimates of the two targets be denoted by $\hat{X}_{o1}$ and $\hat{X}_{o2}$:

$$\hat{X}_{o1} = \begin{bmatrix} \hat{x}_{o1} \\ \hat{v}_{x1} \\ \hat{y}_{o1} \\ \hat{v}_{y1} \end{bmatrix} \quad \hat{X}_{o2} = \begin{bmatrix} \hat{x}_{o2} \\ \hat{v}_{x2} \\ \hat{y}_{o2} \\ \hat{v}_{y2} \end{bmatrix}.$$

The calculated Doppler shift responses at each receiver are shown in Table 4.3.

Table 4.3. Calculated Doppler shift data (two-target, three-receiver case).

	Calculated Doppler Shift –1	**Calculated Doppler Shift -2**
RX1	$h_1(\hat{X}_{o1})$	$h_1(\hat{X}_{o2})$
RX2	$h_2(\hat{X}_{o1})$	$h_2(\hat{X}_{o2})$
RX3	$h_3(\hat{X}_{o1})$	$h_3(\hat{X}_{o2})$

At RX1, Doppler response m_{11} is assigned to target 1 and m_{12} is assigned to target 2. The next step is to optimally assign the responses at RX2 and RX3, since it is not known which response corresponds to which target. For example, at RX2, response m_{21} and m_{22} could have been produced by target 1 and target 2, respectively, or by target 2

and target 1, respectively. The same uncertainty exists at RX3. The number of possible combinations can be enumerated with the formula

$$\text{no. of combinations} = (n_t!)^{n_r - 1}, \tag{4.3}$$

where n_t is the number of targets and n_r is the number of receivers. In this case, with n_t=2 and n_r=3, there are four different possible combinations of the measured Doppler shift data. The four combinations are shown in Table 4.3.

Table 4.4. Combinations of measured Doppler responses for the simultaneous method.

	Combination #1	**Combination #2**	**Combination #3**	**Combination #4**
RX1	m_{11} m_{12}	m_{11} m_{12}	m_{11} m_{12}	m_{11} m_{12}
RX2	m_{21} m_{22}	m_{21} m_{22}	m_{22} m_{21}	m_{22} m_{21}
RX3	m_{31} m_{32}	m_{32} m_{31}	m_{31} m_{32}	m_{32} m_{31}

The problem now is to determine which combination in Table 4.4 corresponds to the calculated Doppler response in Table 4.3. To optimally associate the measurements with the targets and to determine the initial target states, the L-M algorithm is used to minimize the cost (sum-squared error) between each measured Doppler response combination and the calculated Doppler responses. The combination that gives the lowest cost defines the optimal target association, in addition to providing the position and velocity for all targets.

Considering combination 1, denote the two columns of the corresponding response matrix (Table 4.4) as M_1 and M_2, i.e.,

$$M_1[k] = \begin{bmatrix} m_{11}[k] \\ m_{21}[k] \\ m_{31}[k] \end{bmatrix} \quad \text{and} \quad M_2[k] = \begin{bmatrix} m_{12}[k] \\ m_{22}[k] \\ m_{32}[k] \end{bmatrix}. \tag{4.4}$$

Define the corresponding calculated responses as

$$h_{r1}[k] = \begin{bmatrix} h_1(\hat{X}_{o1}) \\ h_2(\hat{X}_{o1}) \\ h_3(\hat{X}_{o1}) \end{bmatrix} \quad \text{and} \quad h_{r2}[k] = \begin{bmatrix} h_1(\hat{X}_{o2}) \\ h_2(\hat{X}_{o2}) \\ h_3(\hat{X}_{o2}) \end{bmatrix}. \tag{4.5}$$

The time variable *k* in the calculated responses has been dropped for notational convenience. The cost to be minimized (for combination 1) is

$$C = C_1 + C_2, \tag{4.6}$$

where the sub-costs C_1 and C_2 are given by

$$C_1 = \sum_{k=0}^{N-1} \left\| M_1[k] - h_{r1}[k] \right\|^2, \tag{4.7}$$

$$C_2 = \sum_{k=0}^{N-1} \left\| M_2[k] - h_{r2}[k] \right\|^2, \tag{4.8}$$

$\|\cdot\|$ denotes the Euclidean norm, and *N* is the number of time steps. Thus,

$$C_1 = \sum_{k=0}^{N-1} \{ [m_{11}[k] - h_1(\hat{X}_{o1})]^2 + [m_{21}[k] - h_2(\hat{X}_{o1})]^2 + [m_{31}[k] - h_3(\hat{X}_{o1})]^2 \}. \tag{4.9}$$

The expression for sub-cost C_2 is derived in a similar manner.

The minimization of the cost *C* is performed with respect to the initial target states $\hat{X}_{o1}$ and $\hat{X}_{o2}$. However, C_1 is a function only of $\hat{X}_{o1}$, and C_2 is a function only of $\hat{X}_{o2}$. Therefore, C_1 and C_2 can be minimized independently.

As seen from (2.29), the L-M iteration is given by

$$\hat{X}_{o_{n+1}} = \hat{X}_{o_n} + (H^T H + \lambda I)^{-1} H^T (z - h(\hat{X}_{o_n})), \tag{4.10}$$

where $\hat{X}_{o_n}$ denotes the estimate of X_o (X_{o1} for C_1 and X_{o2} for C_2) at the *n*th iteration and *I* denotes the 4x4 identity matrix. The variable λ is the constant parameter used in the L-

M calculation and was empirically chosen to be 0.0002 in all simulations throughout this thesis. For minimizing the sub-cost C_1, the variables z, h, and H are defined as

$$z = \begin{bmatrix} M_1[0] \\ M_1[1] \\ \vdots \\ M_1[N-1] \end{bmatrix}_{3N\times 1}, \quad h(\hat{X}_{o1}) = \begin{bmatrix} h_{r1}[0] \\ h_{r1}[1] \\ \vdots \\ h_{r1}[N-1] \end{bmatrix}_{3N\times 1}, \; H = \frac{\partial h}{\partial \hat{X}_{o1}} = \begin{bmatrix} H_{r1}[0] \\ H_{r1}[1] \\ \vdots \\ H_{r1}[N-1] \end{bmatrix}_{3N\times 4} \tag{4.11}$$

where

$$H_{r1}[k] = \frac{\partial h_{r1}[k]}{\partial \hat{X}_{o1}} = \begin{bmatrix} \frac{\partial h_1[k]}{\partial x_1[0]} & \frac{\partial h_1[k]}{\partial v_{x1}} & \frac{\partial h_1[\mathrm{k}]}{\partial \mathrm{y}_1[0]} & \frac{\partial h_1[k]}{\partial v_{y1}} \\ \frac{\partial h_2[k]}{\partial x_1[0]} & \frac{\partial h_2[k]}{\partial v_{x1}} & \frac{\partial h_2[\mathrm{k}]}{\partial \mathrm{y}_1[0]} & \frac{\partial h_2[k]}{\partial v_{y1}} \\ \frac{\partial h_3[k]}{\partial x_1[0]} & \frac{\partial h_3[k]}{\partial v_{x1}} & \frac{\partial h_3[\mathrm{k}]}{\partial \mathrm{y}_1[0]} & \frac{\partial h_3[k]}{\partial v_{y1}} \end{bmatrix}_{3\times 4}, \tag{4.12}$$

and h and H in the above equations are evaluated at the value at the nth iteration ($\hat{X}_{o_n}$).

The entries in the above matrix are obtained by differentiating equation (4.1), where

$$x_1[k] = x_1[0] + v_{x1}kT,$$

$$y_1[k] = y_1[0] + v_{y1}kT, \tag{4.13}$$

$v_{x1} = \dot{x}_1$ and $v_{y1} = \dot{y}_1$ denote constant velocities, and T is the sampling period.

The L-M procedure gives the LSE estimate $\hat{X}_{o1}$ (of target 1 state) for combination 1. Minimization of sub-cost C_2 is performed using the same procedure and gives the LSE estimate $\hat{X}_{o2}$ (of target 2 state) for this combination.

The procedure described above for combination 1 is applied to the remaining 3 combinations. The combination that gives the smallest cost represents the optimal target

association and the best state estimates of the target states. This procedure is applicable to any number of targets and receivers, although the number of combinations grows rapidly.

4.2.2 Example: Multi-Target Case

Two-Target, Two-Receiver Case

To demonstrate the simultaneous method, a second target was added to the scenario considered in the one-target example in Section 4.2.2. When two targets are considered in a two-receiver sensor network, there are only two possible combinations measured Doppler responses, i.e.,

$$\begin{bmatrix} m_{11} & m_{12} \\ m_{21} & m_{22} \end{bmatrix} \quad \text{and} \quad \begin{bmatrix} m_{11} & m_{12} \\ m_{22} & m_{21} \end{bmatrix}.$$

Figure 4.4 shows the plan view of the sensor network and the targets' trajectories. The second target's speed is 140 m/s, and a time duration of 100 s was used with a sampling interval of 1 s.

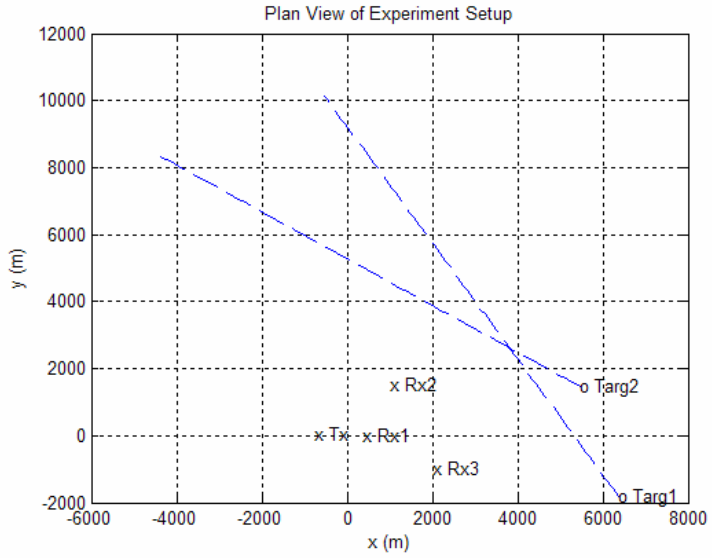

Figure 4.4. Plan view of sensor network and target trajectory via simultaneous method (two-target, two-receiver case).

The actual and estimated target states for target 1 and target 2 were

$$X_{o1} = \begin{bmatrix} 6830.1 \\ -70 \\ -1830.1 \\ 121.24 \end{bmatrix} \text{ and } \hat{X}_{o1} = \begin{bmatrix} 6361.7 \\ -69.355 \\ -1865.7 \\ 121.57 \end{bmatrix},$$

$$X_{o2} = \begin{bmatrix} 5464.1 \\ -100.24 \\ 1464.1 \\ 70 \end{bmatrix} \text{ and } \hat{X}_{o2} = \begin{bmatrix} 5480.3 \\ -100.46 \\ 1477.1 \\ 70.055 \end{bmatrix}.$$

The simultaneous method performed well for these two target states, providing excellent state estimates.

Just as in the sequential method, the simultaneous method may not successfully estimate the target states because of convergence to local minima or failure of the L-M algorithm to converge in a reasonable number of iterations. Statistical properties of success rates and accuracies of the methods are investigated in Section 4.3. One method of increasing the estimation success rate is to add a third receiver. An example of a two-target, three-receiver case is considered next.

Two-Target, Three-Receiver Case

The plan view of the sensor network when another receiver is added is shown in Figure 4.5.

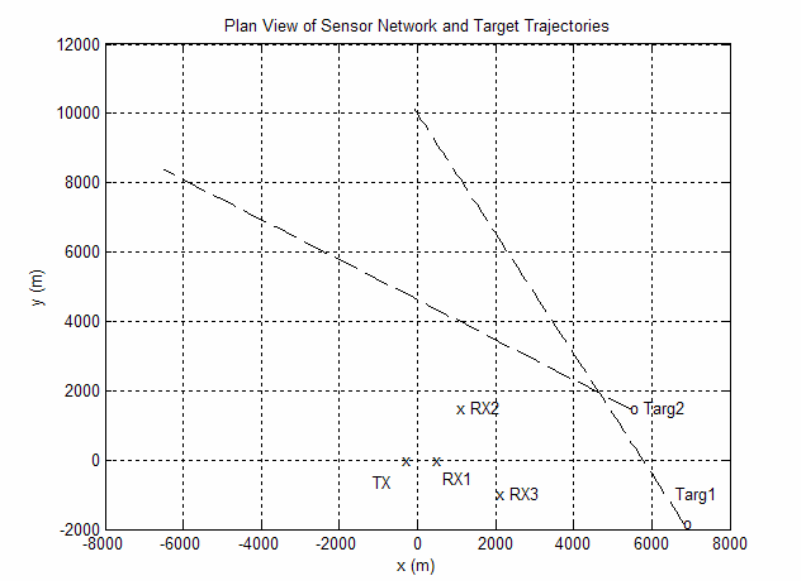

Figure 4.5. Plan view of sensor network and target trajectory via simultaneous method (two-target, three-receiver case).

When two targets are considered in a three-receiver sensor network, there are now four possible combinations of measured Doppler responses, i.e.,

$$\begin{bmatrix} m_{11} & m_{12} \\ m_{21} & m_{22} \\ m_{31} & m_{32} \end{bmatrix}, \begin{bmatrix} m_{11} & m_{12} \\ m_{21} & m_{22} \\ m_{32} & m_{31} \end{bmatrix}, \begin{bmatrix} m_{11} & m_{12} \\ m_{22} & m_{21} \\ m_{31} & m_{32} \end{bmatrix}, \begin{bmatrix} m_{11} & m_{12} \\ m_{21} & m_{22} \\ m_{32} & m_{31} \end{bmatrix}.$$

Results show that combination #1 gives the optimal association for this network setup (i.e., this combination had the lowest of the four costs). The actual and estimated states for target 1 and target 2 for this correct combination are

$$X_{o1} = \begin{bmatrix} 6830.1 \\ -70 \\ -1830.1 \\ 121.24 \end{bmatrix} \text{ and } \hat{X}_{o1} = \begin{bmatrix} 6826 \\ -69.741 \\ -1842.9 \\ 121.38 \end{bmatrix}$$

$$X_{o2} = \begin{bmatrix} 5464.1 \\ -121.24 \\ 1464.1 \\ 70 \end{bmatrix} \text{ and } \hat{X}_{o2} = \begin{bmatrix} 5468.1 \\ -121.43 \\ 1472.4 \\ 69.925 \end{bmatrix}$$

As compared with the two-receiver case, the addition of another receiver to the network improves association results and state estimate accuracy significantly. Figure 4.6 shows the measured versus estimated Doppler responses for the correct combination #1. The numerical results from the cost analysis are corroborated in these plots since there is a near-perfect match between the measured and estimated Doppler responses. Conversely, Figure 4.7 shows the measured versus estimated Doppler responses for one of the three incorrect combinations, which indicates a poor match.

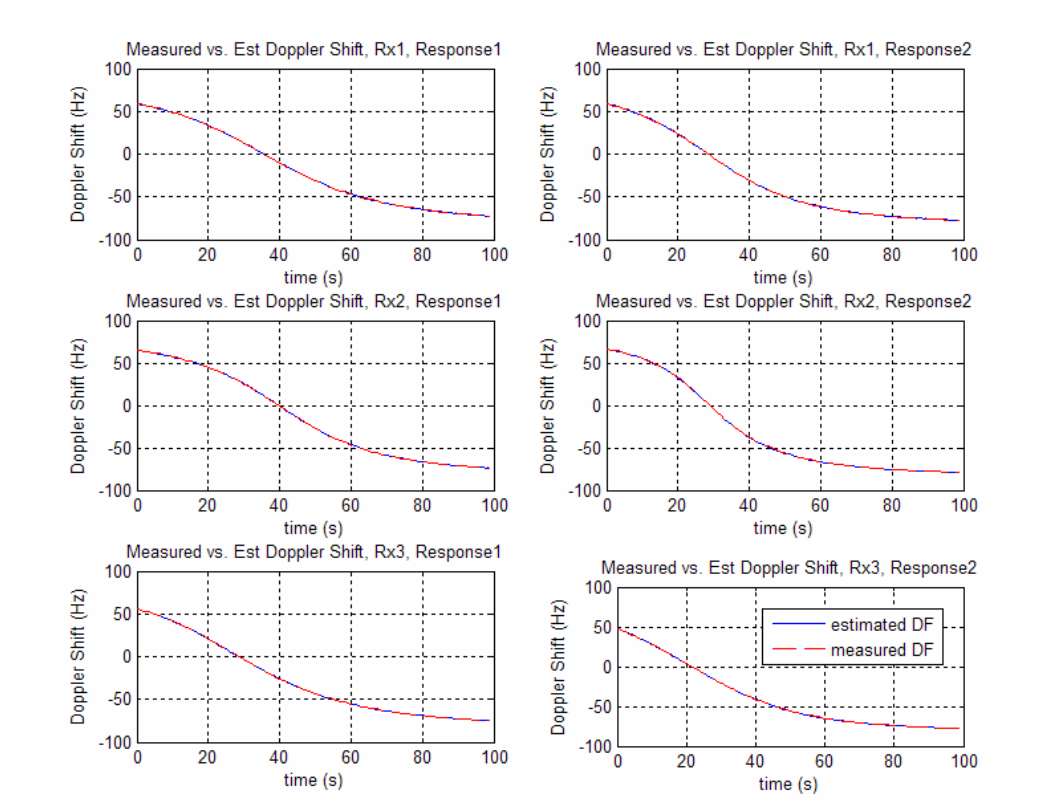

Figure 4.6. Measured versus estimated Doppler shift for the optimal association combination via simultaneous method (two-target, three-receiver case).

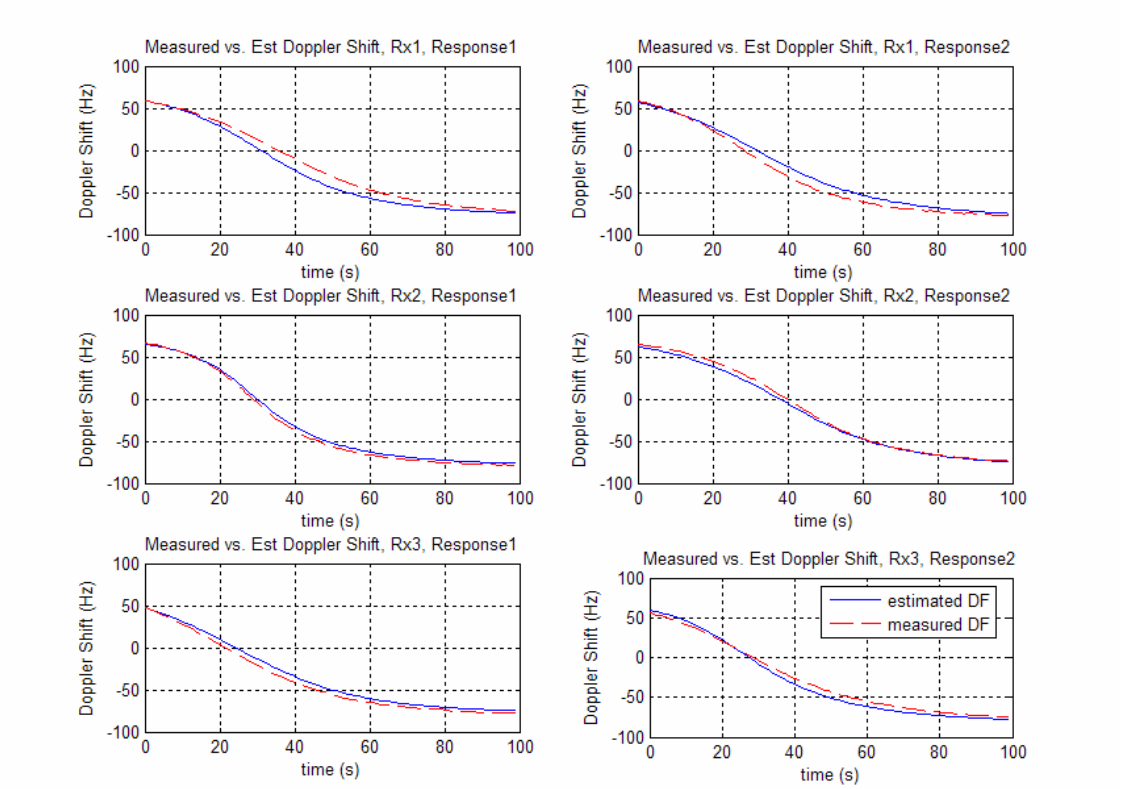

Figure 4.7. Measured versus estimated Doppler shift for an incorrect association combination via simultaneous method (two-target, three-receiver case).

The results from the two-target, three-receiver simulation show that when multiple receivers are offset from the original RX-TX line, the simultaneous method works well. Additionally, if parallel hardware is available, the addition of this third receiver will not significantly increase the computation time since the L-M calculations for each combination can be done independently.

4.3 Monte Carlo Simulation Results

A number of Monte Carlo simulations were conducted to examine how each target tracking and association method performed in realistic scenarios. In all the Monte Carlo runs, quantization noise due to FFT bin size (as discussed in Section 2.4) was

included in the Doppler shift measurements to simulate a realistic system, as discussed in [2]. Thus, for a sampling period of 1 s, the measurement noise was uniformly distributed over the interval (-0.5, 0.5) Hz. However, in more modern systems, this noise could be modeled as SNR-dependent Gaussian noise [19], as discussed in Section 2.4. Using this Gaussian noise model, more accurate state estimation could be achieved. The two-target, two-receiver case was tested for both the sequential and simultaneous method. For each Monte Carlo run, the targets are assumed to be located at polar coordinates (r_i, θ_i), i=1, 2, where the range r_i is normally distributed (mean=5000 m and standard deviation of 1000m) and θ_i is uniformly distributed over $[-\pi, \pi]$. The two statistical measures used for performance evaluation were the mean and standard deviation of state estimation error. In addition, the mean and standard deviation of the target location error (distance between actual and estimated position at the end of the data duration) is also presented.

Initialization of the L-M algorithm was assumed to be done using the grid-aided technique. In an effort to reduce computational runtimes, instead of running a grid-aided search before each full L-M estimate run, the standard deviations of the raw grid-aided *x*- and *y*-position errors (obtained in Chapter 3) were used to form an initial estimate which, in effect, attempts to simulate the results that would have been obtained from a grid-aided search. A hypothetical grid-aided initial guess of *x*- and *y*-position is conjectured by adding zero-mean normally distributed random variables with a standard deviation of approximately 1000 meters to the actual initial position of the target. The standard deviations of the velocity errors in the grid-aided technique were relatively large, therefore arbitrary initial velocity estimates of zero in the *x* and *y* directions were used. Thus, the assumed grid-aided initial guess for the target state was

$$\text{initial guess for target state} = \begin{bmatrix} x_o + (\sigma_{x\_error}) * randn \\ 0 \\ y_o + (\sigma_{y\_error}) * randn \\ 0 \end{bmatrix},$$

where σ_{x_error} and σ_{y_error} denote the error standard deviation in grid-aided estimation (approximately 1000 m each), and *randn* denotes a realization of a zero-mean, unit variance, Gaussian random variable (a built-in MATLAB function).

In addition to presenting the error between the actual and estimated initial states, the Monte Carlo results are also presented in terms of location errors. The location error is the distance between actual and estimated locations of the target, given by

$$\text{location error} = \sqrt{[x(t_f) - \hat{x}(t_f)]^2 + [y(t_f) - \hat{y}(t_f)]^2}\ , \qquad (4.14)$$

where t_f is the final time.

In the sequential method, assuming that the target association is correctly accomplished in steps 1-5, the cost to be minimized (using data from all receivers) for each target is given in (4.2) for the j^{th} target. Upon applying the L-M procedure, if the minimum cost for target j is sufficiently small (smaller than a predetermined threshold value), it can be concluded that this target state has been successfully estimated. In the simultaneous method, the cost to be minimized for each combination includes the sum-squared errors for all responses at all receivers. The costs corresponding to incorrect combinations are usually much higher, often by orders of magnitude, thereby making it relatively straightforward to determine the optimal association. Upon applying the L-M procedure to sub-cost C_j for the j^{th} target (as in (4.7), (4.8)), if the minimum sub-cost C_j is sufficiently small (smaller than a threshold value), it can be concluded that the state of target j has been successfully estimated.

In the Monte Carlo simulations, a successful run was defined as a run in which the L-M procedure converged within the maximum number of iterations allowed (1500 iterations), and gave reasonable state estimates of all targets, based on the knowledge of the true target states (truth-assisted post-processing). In actual implementation, however, it will be necessary to define a cost threshold in order to determine if a solution is a valid state estimate. If reasonable state estimates are obtained for some (but not all) of the targets, it can be defined as a partial success. The cost threshold can be defined based on statistical analysis. The convergence threshold (maximum change in norm of the state estimate from iteration to iteration) for the L-M procedure was set at 10^{-10} %. Results of Monte Carlo simulations for the sequential and simultaneous methods for the two-target, two-receiver case are presented in the next section.

4.3.1 Sequential Method Statistical Results

Fifty Monte Carlo simulation runs were made for the two-target, two-receiver case. A success rate of 68% (34 out of 50) was observed. For simple interpretation, the results from the two targets, which are statistically similar, were combined, which yielded 68 data sets (consisting of successful runs only) for statistical analysis. The bias (mean) and square root mean-squared error (MSE) of the state vector error were

$$bias(\hat{X}_o - X_o) = \begin{bmatrix} -0.061116 \\ 0.047294 \\ -1.1329 \\ 0.018317 \end{bmatrix}, \quad \sqrt{MSE}(\hat{X}_o - X_o) = \begin{bmatrix} 45.977 \\ 0.80143 \\ 38.629 \\ 0.63516 \end{bmatrix}.$$

The average absolute location error and square root MSE of the location error at the end of the data period were: 62.523 m and 47.362 m.

Statistics in x and y direction for the combined target data at the end of the data period are presented in Table 4.5.

Table 4.5. Statistical Monte Carlo results for the sequential method (two-target, two-receiver case).

All units in m	Combined Target Data
Bias ($\hat{x} - x$)	4.621
$\sqrt{MSE}$ ($\hat{x} - x$)	53.095
Bias ($\hat{y} - y$)	0.68049
$\sqrt{MSE}$ ($\hat{y} - y$)	58.048
Average Absolute Location Error	62.523
$\sqrt{MSE}$ of Location Error	47.362

In the successful Monte Carlo runs (68%), perfect target association as well as good tracking performance was obtained. In the unsuccessful cases, all target associations were correct, and one of the target state estimates was often reasonably accurate while the other target state estimate was grossly wrong. Occasionally the L-M algorithm could not find a solution in a reasonable number of iterations, indicated by non-convergence. The unsuccessful (and partially successful) runs were not included in the presented accuracy results. The time duration used was 100 s. The receiver order, which makes a difference in the sequential method, turned out to be important in determining optimal target association and state estimates.

As mentioned previously, it will be necessary to determine the cost threshold for an acceptable target state estimate. Additional Monte Carlo analyses can be performed to find the average cost per response corresponding to good target state estimates (in successful and partially successful cases), as well as the average cost per response

corresponding to incorrect target state estimates. A suitable threshold value can be determined subsequently.

4.3.2 Simultaneous Method Statistical Results

Two-Target, Two-Receiver Case

Fifty Monte Carlo simulation runs were made for the two-target, two-receiver case using the simultaneous method. The observed success rate was 62% (31 out of 50). As in the sequential method, results for the two targets were combined to obtain 62 data sets (consisting of successful runs only) for statistical analysis. The bias and square root mean-squared error (MSE) of the state vector error for the combined data were found to be

$$bias(\hat{X}_o - X_o) = \begin{bmatrix} 0.83762 \\ 0.055106 \\ 1.0837 \\ -0.01865 \end{bmatrix}, \sqrt{MSE}(\hat{X}_o - X_o) = \begin{bmatrix} 38.797 \\ 0.74304 \\ 33.794 \\ 0.58786 \end{bmatrix}.$$

The average absolute location error and square root mean-squared error (MSE) of the location error at the end of the data period were 56.142 m and 46.268 m, respectively. Statistics for combined target estimate errors at the end of the data duration are presented in Table 4.6.

Table 4.6. Statistical Monte Carlo results for the simultaneous method (two-target, two-receiver case).

All units in *m*	Combined Target Data
Bias ($\hat{x} - x$)	0.93362
$\sqrt{MSE}$ ($\hat{x} - x$)	45.175
Bias ($\hat{y} - y$)	1.275
$\sqrt{MSE}$ ($\hat{y} - y$)	52.228
Average Absolute location error	56.142
$\sqrt{MSE}$ of Location Error	46.268

The simultaneous method was successful in 62% of the runs compared to 68% for the sequential case. The errors are similar to those obtained by the sequential method. Similar to the simultaneous method, the sequential method uses the data from all receivers to perform the least squares minimization (as described in Section 4.1.1 (4.2)), although the target association is performed sequentially. Therefore, the accuracy is expected to be similar.

Two-Target, Three-Receiver Case

In an attempt to increase the success rate and accuracy, the effect of adding a third receiver was studied. Fifty Monte Carlo simulation runs were made for the two-target, three-receiver case using the simultaneous method. The observed success rate was 78% (34 out of 50). As in the previous cases only successful runs were included in the statistical analysis. The bias and square root mean-squared error (MSE) of the state vector error for the combined data were found to be

$$bias(\hat{X}_o - X_o) = \begin{bmatrix} 3.104 \\ -0.080863 \\ 4.1787 \\ -0.014942 \end{bmatrix}, \sqrt{MSE}(\hat{X}_o - X_o) = \begin{bmatrix} 18.016 \\ 0.38032 \\ 22.78 \\ 0.30881 \end{bmatrix}.$$

The average absolute location error and square root mean-squared error (MSE) location error at the end of the data period were 31.859 m and 23.315 m, respectively. Statistics for combined target estimate errors at the end of the data duration are presented in Table 4.7.

Table 4.7. Statistical Monte Carlo results for the simultaneous method (two-target, three-receiver case).

All units in *m*	Combined Target Data
Bias ($\hat{x} - x$)	-4.9014
$\sqrt{MSE}$ ($\hat{x} - x$)	31.639
Bias ($\hat{y} - y$)	2.6994
$\sqrt{MSE}$ ($\hat{y} - y$)	23.217
Average Absolute Location Error	31.859
$\sqrt{MSE}$ of Location Error	23.315

The simultaneous method with three receivers was successful in 78% of the runs compared to 62% for the simultaneous method with two receivers. The average absolute location error and the square root MSE of location error are significantly smaller than the two-receiver case.

Additional Monte Carlo analyses can be performed to find the average cost per response corresponding to good target state estimates (in successful and partially successful cases), as well as the average cost per response corresponding to incorrect target state estimates. A suitable threshold value can be determined subsequently. The cost for incorrect combinations is much higher (by orders of magnitude) than the cost for the optimal combination; therefore incorrect combinations can be discarded in a relatively straightforward manner.

The computational complexity of the sequential and simultaneous methods is analyzed in the next section.

4.4 Computational Complexity Analysis

This section studies the computational requirements of the sequential and simultaneous methods. The main computational burden in these methods is the L-M iterations (which requires computation of Doppler shift and its partial derivatives for all time steps, in addition to a 4x4 matrix inversion). Hence, the number of L-M procedures required in each method is a suitable quantifying measure of computational complexity. The complexities were calculated for the two- and three- receiver cases in both the sequential and simultaneous methods. If multiple transmitters and a single receiver are used instead of multiple receivers and single transmitter, the computational complexities do not change.

4.4.1. Sequential Method Computational Complexity

As described in Section 4.1, in the first step, the L-M algorithm is executed n_t times (where n_t is the number of targets) in order to generate n_t target state estimates. Using data from only RX1, each estimate had three additional ghost targets because of symmetry. After correct target association for the other receivers is completed via our full blocking procedure with the help of measured data at the other receivers, the L-M algorithm is executed another n_t times (once for each target), now incorporating the data from all receivers to achieve a better state estimate. Hence, the number of L-M procedures is $2*n_t$. However, the sequential method also investigates the effect of changing the receiver order. Therefore, the method described above must be executed

once for each receiver order, that is, (n_r!) times, where n_r is the number of receivers. The final computation complexity for the sequential method can be quantified as

$$\text{computational complexity} = 2*(n_r!) * n_t \tag{4.15}$$

Thus the computational complexity is a linear function of the number of targets, but grows rapidly with the number of receivers.

4.4.2. Simultaneous Method Computational Complexity

The simultaneous method was based on the idea of examining all possible combinations of the measured data. Let *ncombo* be the number of possible combinations of measured data. As seen in (4.3),

$$ncombo = (n_t!)^{n_r-1}.$$

For each combination, there were n_t number of sub-costs, and there was one L-M procedure per sub-cost. Hence, the total number of L-M procedures can be generalized as

$$\text{computational complexity} = n_t * (n_t!)^{n_r-1}. \tag{4.16}$$

Figure 4.8 illustrates the computational complexity as a function of n_t, for n_r=2, 3, respectively, for the sequential and simultaneous methods.

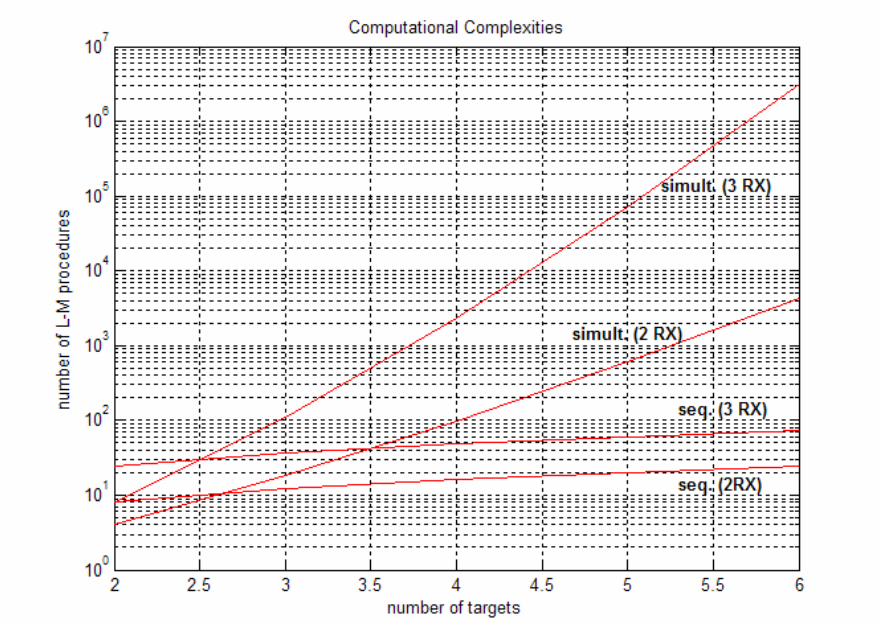

Figure 4.8. Computational complexities for sequential and simultaneous methods.

For the simultaneous method, the computational complexity increases rapidly with the number of targets and the number of receivers.

4.5. Time Duration Requirements for Target State Estimation

From intuition, it is expected that a longer data collection time duration will most likely result in a better state estimate since there is more information available. A study was conducted to determine how much time is needed to accurately estimate a target's state for a typical tangential trajectory of r=5000 at angles of $\theta = \frac{\pi}{6}, \frac{\pi}{3}$ (two target case). The Doppler shift measurement included quantization noise. The location errors were compared for both the sequential and simultaneous methods. Figures 4.9-4.12 show how the location errors are affected by the length of data collected. The results are for the two-receiver, two-target scenario in both methods.

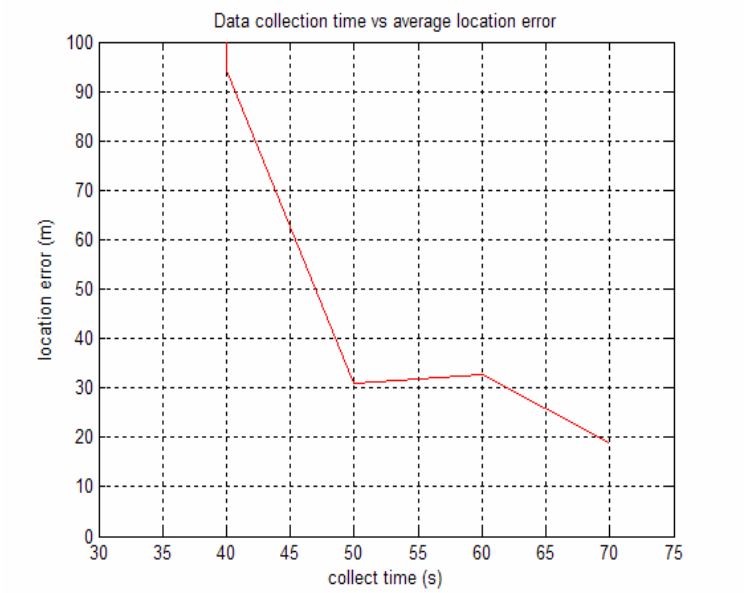

Figure 4.9. Data collection time vs. average location error for the sequential method.

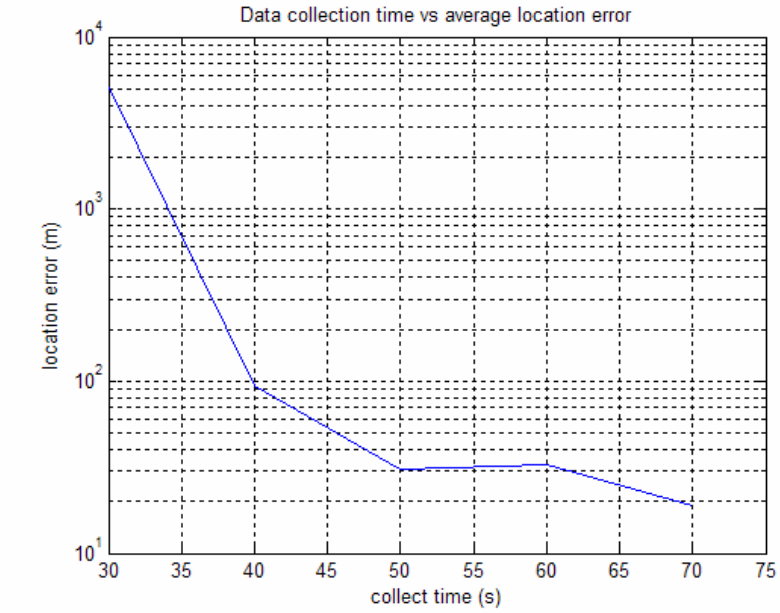

Figure 4.10. Data collection time vs. average location error for the sequential method (semilog-y plot).

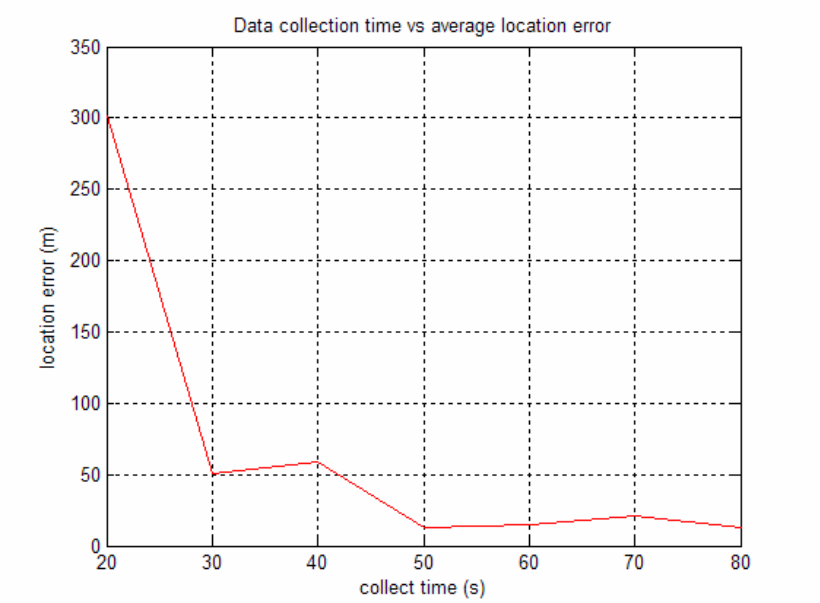

Figure 4.11. Data collection time vs. average location error for the simultaneous method.

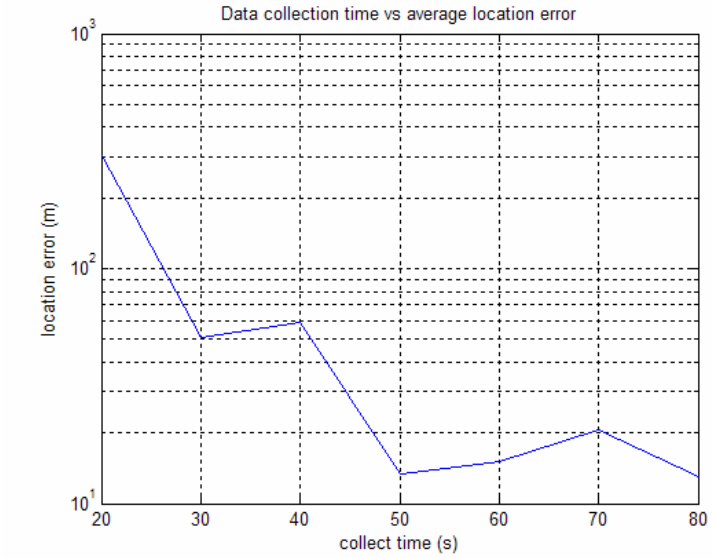

Figure 4.12. Data collection time vs. average location error for the simultaneous method (semilog-y plot).

For the case considered, the sequential method required a longer collection time than the simultaneous method. For the sequential method, reasonable state estimates were obtained after 50 s, whereas it took the simultaneous method only 30 s to achieve a

similar location error. However, both methods eventually achieve small location errors when sufficiently long data collection time is available.

4.6 Existence of Local Minima

While performing Monte Carlo simulations (Section 4.3), it was found that in most of the unsuccessful runs, the L-M algorithm converged, but to grossly incorrect state estimates for one of the targets. This suggests the existence of local minima. To investigate this further, an example case was considered. Figure 4.13 shows the plan view and trajectories in a two-target, two-receiver setup where target 2 has converged to a completely incorrect state estimate, although Doppler response errors at both receivers were included in the cost function (as in (4.2)). The actual and estimated states for target 2 are

$$X_{o2} = \begin{bmatrix} -3705.3 \\ 139.02 \\ -2916.8 \\ -16.553 \end{bmatrix} \text{ and } \hat{X}_{o2} = \begin{bmatrix} 922.8 \\ -117.03 \\ -4637.4 \\ 76.19 \end{bmatrix}$$

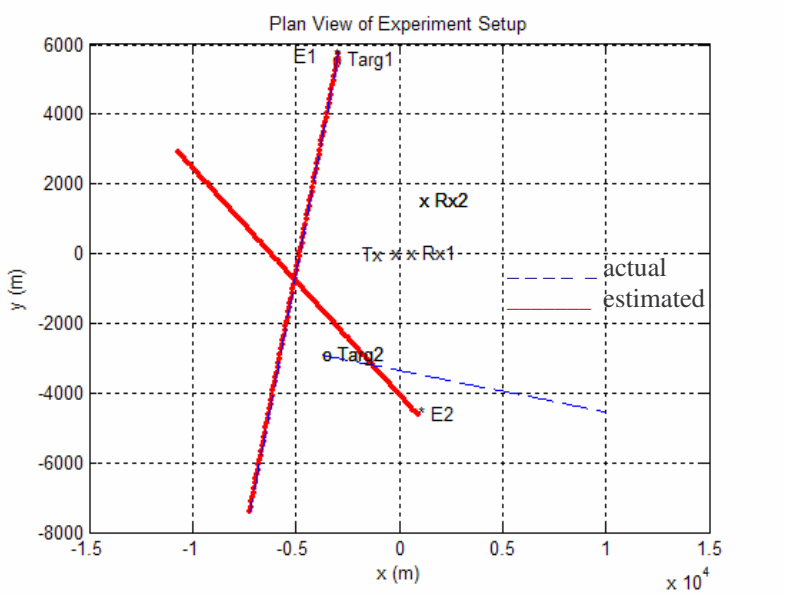

Figure 4.13. Plan view of experiment setup showing how target 2 converged to an incorrect target state.

Figure 4.14 shows the cost function plotted in the neighborhood of the true position, while Figure 4.15 shows the cost function plotted in the neighborhood of the estimated position for target 2. The cost function consists of the sum of costs at the two receivers. These plots clearly show the existence of local minima at two completely different positions. The cost for the incorrect state estimate (local minimum) is 97.776, while the cost for the actual state (global minimum) was 15.802. The cost for the actual state would be zero in the absence of noise. The incorrect state estimates are local minima and have higher costs than the optimal state estimate. A cost threshold (0.4 to 0.5 Hz^2 per sample for the noise level considered) could be used to determine if the solution obtained is a local minimum.

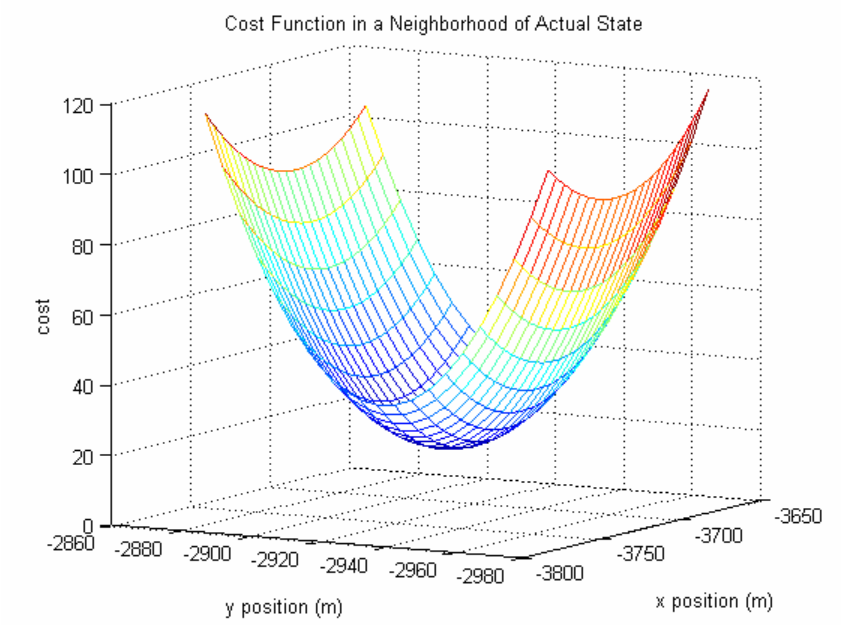

Figure 4.14. Plot of cost function in a neighborhood of the actual state.

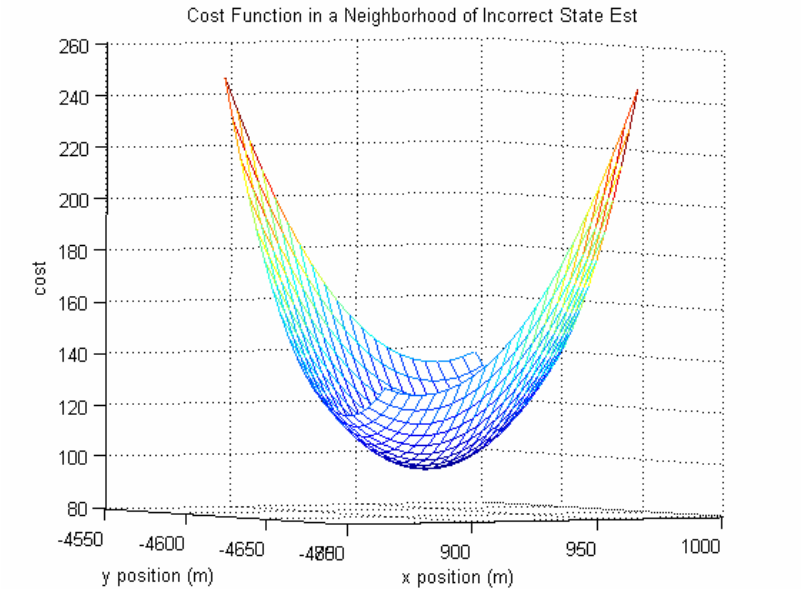

Figure 4.15. Plot of cost function in a neighborhood of the incorrect state estimate.

CHAPTER 5

CONCLUSIONS AND FUTURE WORK

The research presented in this thesis focused on the problem of target tracking and association using Doppler shift as the sole measurement in a two-dimensional setting. A passive tracking approach exploiting preexisting FM radio transmissions was considered. An NLSE batch processing technique called the Levenberg-Marquardt algorithm was used to estimate the target states. For a single transmitter-receiver scenario, it was analytically shown that four distinct target trajectories produce identical Doppler responses because of symmetry. However, this ambiguity could be broken by adding one more correctly chosen receiver. Equivalently, instead of adding another receiver, another transmitter could be added to help break this ambiguity while not changing any of the analysis or methods. A grid-aided search technique was proposed in an attempt to obtain better starting values for the L-M iterations.

For multi-target tracking and association, two methods, “sequential” and “simultaneous,” were proposed. The terms “sequential” and “simultaneous” refer to the way that target association was performed. In our examples, the L-M algorithm was used as the core parameter estimation technique. If a different parameter estimation algorithm was used, the simulation results might be different. The performance of the two methods was analyzed via Monte Carlo simulations. Results showed that both methods gave results with similar accuracy when two receivers were used to estimate parameters for two targets. For the simultaneous method, the addition of a third receiver significantly improved the success rate as well as accuracy results. The simultaneous method

represents an optimal target association and state estimation method, and is expected to perform at least as well as or better than the sequential method. A brief computational complexity study comparing the sequential and simultaneous methods was conducted. The computational complexity grows linearly with the number of targets for the sequential method, but grows rapidly for the simultaneous method. The effect of data collection time was also investigated. The sequential method required a longer collection time than the simultaneous method.

Since the simulations presented in this research did not consider the z-direction, namely altitude, a further extension of this thesis could be to incorporate these methods into a three-dimensional system. Additionally, it would be interesting to study the effect of maneuvering targets and how the algorithms would change depending on their unpredictable trajectories. Finally, a logical extension of this research would be to use the state estimates calculated from these algorithms to initiate a real-time track maintenance method, such as the extended Kalman filter.

REFERENCES

[1] A. H. Taylor, L.C. Young, and L.A. Hyland, "Systems for detecting objects by radio," US Patent No. 1,981,884, June 13 1933.

[2] P.E. Howland, "Television Based Bistatic Radar," PhD Thesis. University of Birmingham, UK, 1997.

[3] H.D. Griffiths and C.J. Baker, "Passive coherent location radar systems. Part 1: Performance prediction," *IEE Proc.-Radar Sonar Navig*., vol. 152, no. 3, pp. 153-159, June 2005.

[4] L.M. Ehrman and A.D. Lanterman, "Automated Target Recognition Using Passive Radar and Coordinated Flight Models," *Automatic Target Recognition XIII, Proc*. SPIE 5094, April 2003.

[5] B. Mojarrabi, J. Homer, K. Kubik, I.D. Longstaff, and J. Palmer, "Analytical solution for target location using bistatic multi-transmitter and multi-receiver techniques," Proceedings of the International Conference on Radar, pp. 433 – 436, September 2003.

[6] M. Cherniakov, D. Nezlin and K. Kubik, "Air target detection via bistatic radar based on LEOS communication signals," *IEE Proc.-Radar Sonar Navig*., vol. 149, no. I, pp.33-38, February 2002.

[7] A. P. Whitewood, B. R. Muller, H. D. Grifiths, and C. J. Baker, "Bistatic Synthetic Aperture Radar with Application to Moving Target Detection" *Proceedings of IEEE Radar 2003*, pp. 529-534, September 2003.

[8] L. Ehrman, "An Algorithm for Automatic Target Recognition Using Passive Radar and an EKF for Estimating Aircraft Orientation," PhD Thesis, Georgia Institute of Technology, 31 October 2005

[9] A. Price, *Instruments of Darkness – The Struggle for Radar Supremacy*. William Kimbler and Co. Ltd., pp. 216-218, 1967.

[10] J. Baniak, G. Baker, A. Cunningham, and L. Martin "Silent Sentry Passive Passive Surveillance" Lockheed-Martin publication, 7 June 1999.

[11] A.D. Lanterman, "Tracking and recognition of airborne targets via commercial television and FM radio signals", in *Acquisition, Tracking, and Pointing XIII, Proc.* SPIE 3692, pp. 189-198, April 1999.

[12] P.E. Howland, D. Maksimiuk, and G. Reitsma, "FM radio based bistatic radar," *IEE Proc.-Radar Sonar Navig*., vol. 152, no. 3, June 2005.

[13] T. Xiaoming, H. You, D. Shijia, and N. Jinlin, "Doppler Compensation for Passive Coherent Location", ICSP '02 Proceedings, pp. 1457-1460.

[14] W.C. Li, P. Wei, and X. Xiao, "TDOA and T^2/R radar based target location method and performance analysis," *IEE Proc.-Radar, Sonar and Navigation.,* vol. 152, issue 3, pp. 219-223, June 2005.

[15] FMQ FM Radio Database Query. 13 March 2007. <http://www.fcc.gov/mb/audio/fmq.html>

[16] W.D. Blair, "Parameter Estimation," Georgia Tech Research Institute, short course notes.

[17] P.E. Howland, "Passive Tracking of Airborne Targets Using Only Doppler and DOA Information" *IEE Colloquium on Algorithms for Target Tracking*, pp. 37-39, 16 May 1995.

[18] P. E. Howland, "Target tracking using television-based bistatic radar," *IEE Proc.-Radar, Sonar and Navigation,* vol. 146, no. 3, June 1999.

[19] G. Morris, *Airborne Pulsed Doppler Radar.* Artech House, Inc., pp. 229-230, 1988.